Engineering Structures 314 (2024) 118306

Contents lists available at ScienceDirect

Engineering Structures

journal homepage: www.elsevier.com/locate/engstruct

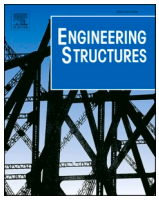

Behavior of steel fiber-reinforced coal gangue concrete beams under impact load

Bin Cai [a], Shengshuai Lu [a], Feng Fu [b,*]

[a] School of Civil Engineering, Jilin Jianzhu University, Changchun 130118, Jilin, China
[b] Department of Engineering, School of Science & Technology, City, University of London, Northampton Square, London EC1V 0HB, UK

ARTICLE INFO

Keywords:
Coal gangue
Steel fiber
Impact resistance
Finite element
LS-DYNA

ABSTRACT

In order to promote the use of new sustainable steel fibers (SF) reinforced coal gangue aggregates (CGA) concrete, impact tests were performed in this paper. The impact resistance of steel fiber-reinforced coal gangue concrete was investigated using a self-developed drop-weight facility. The test variables were the CGA replacement rate (0 %, 50 %, and 100 %), the SF volume content (0 %, 0.75 %, and 1.5 %), and the drop height of the drop-weight (0.5 m and 1.0 m). Using 15 kg of hard steel as a drop-weight, the drop-weight impact test was performed on steel fiber-reinforced coal gangue concrete beams with a span of 300 mm; the damage pattern, impact reaction force-time, displacement-time relationships, and energy absorbed by steel fiber-reinforced coal gangue concrete beams were studied. The test shows that, compared with natural aggregate, CGA reduces concrete's static mechanical properties and impact resistance, and adding SF improves the static mechanical properties and impact resistance of coal gangue concrete. As the CGA replacement rate increased from 0 % to 50 % and 100 %, the reaction force of impact of the specimens decreased by 2.54 %– 6.06 % and 3.69 %– 12.33 %. The SF volume content was increased from 0 % to 0.75 % and 1.5 %, and the reaction force of impact of the specimens was increased by 23.05 %– 32.34 % and 72.27 %– 81.84 %, respectively. The impact resistance of steel fiber-reinforced concrete beams under impact loading was investigated numerically using a nonlinear explicit finite element model in LS-DYNA. The Finite Element results were validated with experimental results. Based on the validated finite element model, a parametric study was carried out to investigate the effects of coal gangue replacement rate, steel fiber volume content, and drop height of the drop weight on the behavior of the beams. This study might provide a basis for the future engineering project applications of steel fiber-reinforced coal gangue concrete under impact conditions.

1. Introduction

Coal gangue is industrial waste generated during coal mining in mines and accounts for about 10 % of coal production [1,2]. Massive accumulation of coal gangue is a severe problem developed and developing countries face. Coal gangue waste not only occupies land but also pollutes soil and groundwater within a radius of 3–5 km around it, and the accumulation of waste seriously threatens the ecological environment, human health, and safety [3–5]. Therefore, it is crucial to improve the utilization rate of coal resources. Using coal gangue instead of natural gravel to form concrete can consume a certain amount of gangue [3–6]. It is of great positive significance to protect the ecological environment, reduce industrial energy consumption, develop environmentally friendly building materials, and reduce the cost of concrete [3,7–9].

Although replacing coarse aggregate in concrete with coal gangue aggregate has many positive aspects, it must also meet specific requirements in terms of mechanical properties and durability [10–13,43,44]. Yao et al. showed that using gangue to replace coarse aggregate in concrete is feasible [7]. Zhou et al. showed that the compressive strength of coal gangue concrete with different gangue replacement ratios meets the design requirements of C30 strength class concrete [14]. Qiu et al. [15] developed a freeze-thaw damage evolution model for coal gangue. Ma et al. [13] found that coal gangue as coarse aggregate in alkaline slag concrete has high compressive strength and good durability. However, coal gangue as a lightweight aggregate has high water absorption and low strength, so the mechanical properties and durability of coal gangue concrete are worse than those of ordinary concrete under the same conditions [16–18]. Although the mechanical properties of coal gangue

* Corresponding author.
E-mail address: feng.fu.1@city.ac.uk (F. Fu).

https://doi.org/10.1016/j.engstruct.2024.118306
Received 24 February 2024; Received in revised form 28 April 2024; Accepted 27 May 2024
Available online 4 June 2024

concrete are less than those of concrete with natural aggregate, coal gangue concrete can still be used in practice [9].

Currently, the application of coal gangue concrete is limited due to its insufficient strength. Compared with ordinary concrete, adding steel fibers to concrete is the method to make up for coal gangue concrete's lack of strength. Steel fibers added to concrete can effectively improve concrete's tensile strength, deformability, crack resistance, and durability [19]. Related studies have shown that adding steel fibers to coal gangue concrete can improve the compressive strength, flexural strength, splitting tensile strength, and durability of coal gangue concrete [20]. The addition of steel fibers to coal gangue concrete can optimize its internal structure and reduce concrete pores, which is beneficial to the frost resistance of concrete [16]. The above results are based on static tests. Many tests have revealed that steel fibers can improve the impact resistance of concrete [21–30]. Hao et al. found that steel fibers can improve the static mechanical properties and impact resistance of concrete beams [22]. Omidinasab et al. investigated the mechanical and impact resistance of steel fibers-reinforced recycled concrete, and the results showed that recycled aggregates had a negative effect on concrete's mechanical and impact resistance. However, steel fibers were able to neutralize this negative effect [23]. Moghadam et al. found that steel fibers have a beneficial effect on improving the flexural and impact resistance of slabs [24]. Zhuang et al. studied the dynamic mechanical properties of steel fibers-reinforced self-compacting concrete (SFRSCC) after high temperatures, and the results showed that steel fibers improved the dynamic mechanical properties of SFRSCC [25]. Abid et al. conducted a repeated impact test with steel fiber-reinforced self-compacting concrete. They investigated the effect of fiber volume content, weight, and drop height on the impact strength of steel fiber-reinforced self-compacting concrete [27]. Almusallam et al. investigated the impact strength of hybrid fiber-reinforced concrete slabs and showed that hybrid fibers significantly reduced the size of the damage zone and prevented the occurrence of damage [28]. Almusallam et al. investigated the behavior of hybrid fiber-reinforced concrete (HFRC) beams under quasi-static loading and projectile impact [30].

The impact resistance of steel fiber concrete is a new area of interest that previous researchers have less studied. Previous researchers have accurately predicted the mechanical properties of concrete beams by Artificial Neural Networks and GA-BPNN Machine Learning [45,46]. In addition, finite element analysis is an effective method for studying the impact resistance of steel fibers-reinforced coal gangue concrete beams [31–38]. Derseh et al. modeled and performed a nonlinear analysis of reinforced concrete beams using LS-DYNA to evaluate the response of reinforced concrete beams under impact loading [31]. Pham et al. simulated the dynamic response of reinforced concrete beams under drop-weight impact using LS-DYNA, impact force, mid-span deflection wave, and crack mode were obtained, which were in good agreement with the test results [32]. Abadel et al. used LS-DYNA to simulate the dynamic behavior of hybrid fiber-reinforced concrete (HFRC) slabs subjected to high-velocity projectile impact. The model could accurately predict the depth of penetration, crater size, impact force, and energy absorbed by the specimen of HFRC slabs subjected to projectile impact [38]. Previous numerical studies have shown that LS-DYNA can accurately model the impact performance of concrete beams. However, there are few studies on the finite element model of steel fiber-reinforced coal gangue concrete beams.

In this paper, the CGA replacement rate (0 %, 50 %, and 100 %), the SF volume content (0 %, 0.75 %, and 1.5 %), and the drop height of the drop-weight (0.5 m and 1.0 m) as variables, and the impact resistance of steel fiber-reinforced coal gangue concrete beams were also investigated using a self-developed drop-weight facility. Failure modes, impact reaction force-time, displacement-time relationships, and energy absorbed by SFCGC during impact with a dropped load were analyzed. Based on the test results, an explicit nonlinear finite element model of the SFCGC beam was created using LS-DYNA software developed by Livermore Software Technology Corporation (LSTC), a self-programmed Python script was used to create the steel fiber model in the FEM of an SFCGC beam. The model was analyzed to verify the accuracy of the created finite element model. In addition, a parametric study of the impact resistance of SFCGC beams was conducted to analyze in more detail the effects of CGA replacement rate (0 %, 20 %, 40 %, 60 %, 80 %, and 100 %), the SF volume content (0 %, 0.5 %, 1.0 %, and 1.5 %) and the drop height of the drop-weight (0.5 m, 0.75 m, and 1.0 m) on the impact resistance of SFCGC beams.

Table 1
Material Properties.

Materials	Properties
Cement	Ordinary silicate cement type P.O 42.5 was used for this test. Compressive strength was 22 MPa (3d) and 43 MPa (28d). The density was 3.1 kg/m^3.
Sand	Ordinary river sand with a bulk density of 2600 kg/m^3 and a fineness modulus 2.94 is classified as medium sand.
Natural aggregate (NA)	Ordinary gravel. Particle gradation is 5–25 mm; apparent density is 2850 kg/m^3 .
Coal gangue aggregate (CGA)	Particle gradation is 5–25 mm; apparent density is 2106 kg/m^3; water absorption is 8.7 %. The chemical composition is shown inTable 2.
Steel fiber	Hooked-end steel fibers are 35 mm long, 0.75 mm in diameter, circular cross-section, and tensile strength 900 MPa.
Water	Ordinary tap water.
Water- reducing agent	Improvement of concrete compatibility.

2. Experimental tests

2.1. Test materials

Table 1 shows the specific properties of the raw materials used for the concrete samples. The chemical composition of coal gangue is given in Table 2. Natural aggregate, coal gangue aggregate, river sand, and hooked-end steel fibers used in concrete are shown in Fig. 1.

2.2. Mix proportion

In order to study the effect of CGA and SF on the impact resistance of SFCGC, the first use of 50 % and 100 % replacement rate of CGA instead of crushed stone, and then mixed with 0.75 % and 1.5 % admixture volume of steel fiber to change the concrete, respectively. The mix proportions of coal gangue concrete are shown in Table 3. The concrete samples are divided into nine groups according to the type of aggregate and the volume content of steel fibers, where the sample group number CG stands for coal gangue. The number after CG indicates the coal gangue replacement rate, while F stands for steel fibers, and the number after F indicates the volume content of steel fibers. For example, CG50-F0.75 represents concrete with a 50 % CGA replacement rate, 0.75 % SF volume content, etc.

The process of concrete preparation is shown in Fig. 2.

2.3. Testing program

2.3.1. Test procedure

The impact resistance of SFCGC beams was evaluated by the recommended procedure for the Measurement of Properties of Fiber Reinforced Concrete (ACI 544.2R-89) [39], and impact tests were performed using a self-developed drop-weight facility. Two drop heights (0.5 m and 1.0 m) were used for the repeated impact tests. Table 4 describes the test standards [39,40], number of specimens, curing age, and specimen size used in this study. The concrete specimens were prepared with reference to the Standard for test method of performance on ordinary fresh concrete (GB/T50080–2016) [41], and a total of 54 cubic specimens and 18 beams were prepared with dimensions of

Table 2
Chemical composition of coal gangue (%).

SiO_2	Al_2O_3	Fe_2O_3	FeO	Na_2O	MgO	K_2O	TiO_2	P_2O_5	MnO
48.76	29.51	8.02	7.35	1.85	2.03	1.54	0.49	0.25	0.2

Fig. 1. Materials.

100 × 100 × 100 mm and 100 × 100 × 400 mm.

2.3.2. Loading method and instrumentation

A self-developed instrumented drop-weight test facility (Fig. 3) was used to carry out the drop-weight impact test by ACI 544.2R-89 [39]. Because the specimen cracked at the first drop, the first cracking strength value and the high scatter of the present data from the impact test are not discussed in this paper. A high-speed video camera and a rapid response meter were used to record the damage process, the displacement, and the reaction force of impact of the specimen under impact load during the repeated impact tests (Fig. 3). The time-dependent reaction force of impact, displacement over time, and corresponding damage patterns of the SFCGC beams were obtained, compared, and discussed. Based on the experimental data, the energy absorption and Ratio of absorbed energy of SFCGC beams were calculated. Two stainless steel rails were mounted in the drop-weight facility; the specimen was placed directly under the rails to allow the drop-weight to fall vertically into the center of the beam. Two load cells were fixed to the solid floor with a spacing of 300 mm between them. The base was placed over the pressure sensor, and then a 100 × 100 × 400 mm specimen was placed on the base and secured with a clamping device. The data acquisition system recorded the data of the pressure sensor at a frequency of 2 kHz. The displacements were obtained using the digital image correlation (DIC) method, which has the advantages of high accuracy, non-contact measurement, and no special environmental requirements compared to traditional contact measurement methods. When analyzing the data, the displacement of the beam at the fulcrum was taken into account to determine the actual central displacement.

2.4. Impact energy calculation

The drop-weight is released and falls along the guide rail before the impact with the friction of the guide rail loss part of the energy; after the

Table 4
Test standard and specimen size.

Test	Number of Specimens	Test standard	Specimen size (mm)	Curing age (Days)
Cube compressive Strength	27	GB/T50081-2019	100 × 100 × 100	28
Splitting tensile strength	27	GB/T50081-2019	100 × 100 × 100	28
Impact resistance	18	ACI 544.2R-89	100 × 100 × 400	28

Table 3
Mixture compositions (Unit: kg/m^3).

Mix ID	Cement	NA	CGA	Sand	Water	WA	SF	W/C	f_{cu} (MPa)	f_{sp} (MPa)
CG0-F0	470	1220	0	830	163	4	0	0.35	56.57	3.26
CG0-F0.75	470	1220	0	830	163	4	0.75	0.35	58.24	3.53
CG0-F1.5	470	1220	0	830	163	4	1.5	0.35	59.10	3.71
CG50-F0	470	610	474	830	163	4	0	0.35	52.07	3.05
CG50-F0.75	470	610	474	830	163	4	0.75	0.35	53.27	3.32
CG50-F1.5	470	610	474	830	163	4	1.5	0.35	54.28	3.49
CG100-F0	470	0	948	830	163	4	0	0.35	49.67	2.84
CG100-F0.75	470	0	948	830	163	4	0.75	0.35	50.84	3.17
CG100-F1.5	470	0	948	830	163	4	1.5	0.35	51.11	3.30

Note: NA= Natural aggregate; CGA = Coal gangue aggregate; WA = Water-reducing agent; SF = Steel fiber; f_{cu}= Cube compressive Strength; f_{sp}= Splitting tensile strength

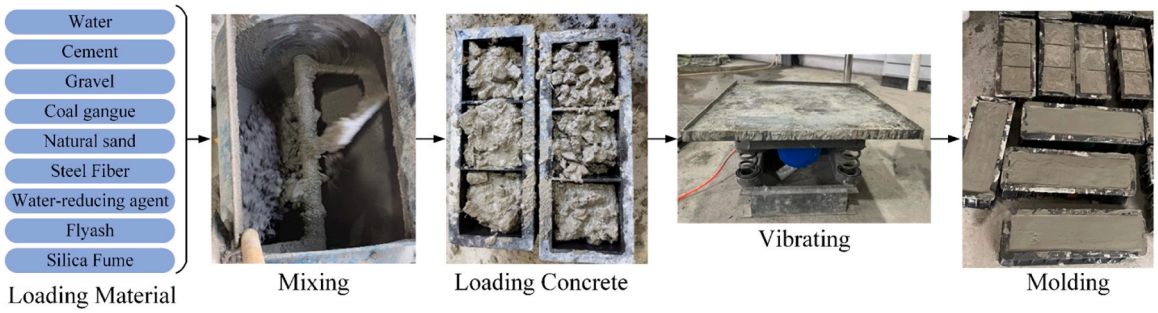

Fig. 2. The production process of steel fiber-reinforced coal gangue concrete.

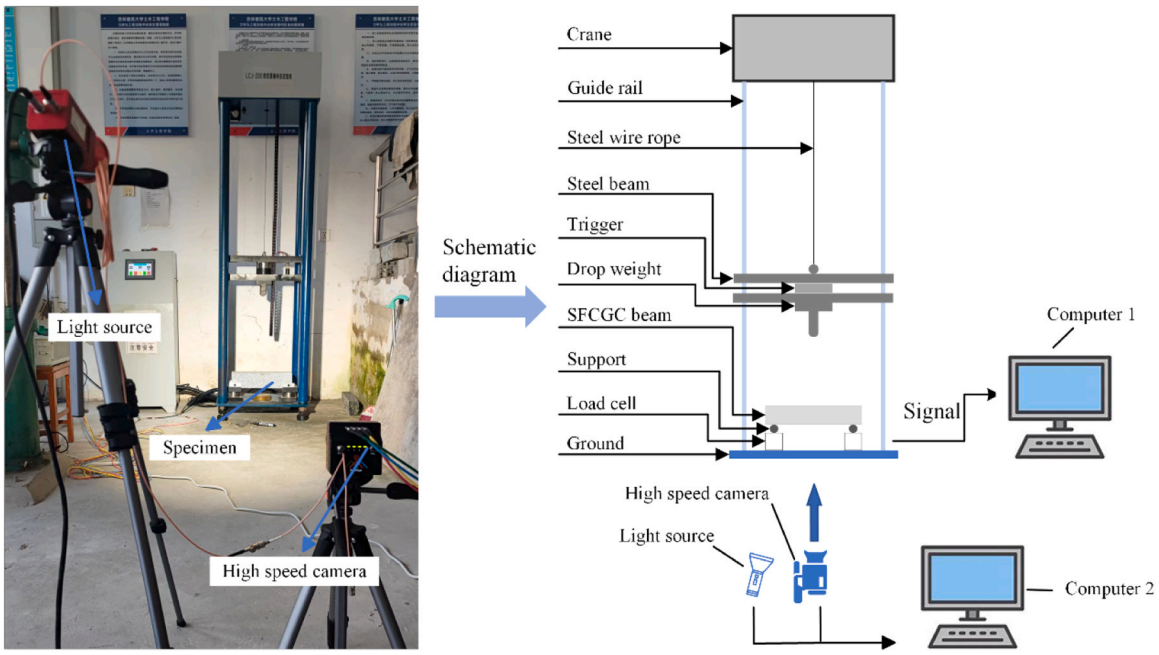

Fig. 3. Schematic diagram of drop-weight impact facility and DIC equipment.

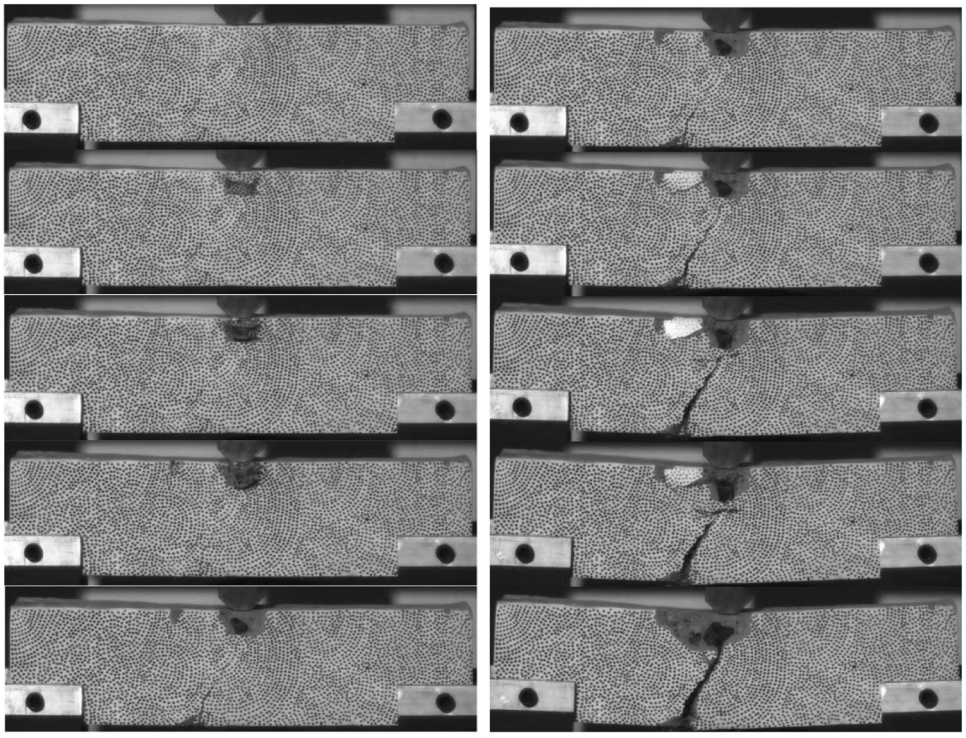

Fig. 4. Destruction process of steel fiber-reinforced coal gangue concrete beams: (a) First impact; (b) Second impact.

sample absorbs the impact part of the energy, the other part of the transfer to the drop-weight facility through the support, the input energy U_i as shown in Eq. (1):

$$U_i = \mathrm{mgH} = \frac{1}{2}\mathrm{mv}_0^2 + U_\mathrm{d} = U_\mathrm{k} + U_\mathrm{f} + U_\mathrm{d} \tag{1}$$

Where U_i is the gravitational potential energy of the drop-weight, m is the mass of the drop-weight, g is the gravitational acceleration of the drop-weight, H is the drop height of the drop-weight, U_d is the frictional energy lost during the fall of the drop-weight, U_k is the energy absorbed by the specimen, and U_f is the energy transferred to the support and consumed by the rebound of the drop-weight. Absorbed energy U_k is calculated according to Eq. (2):

$$U_\mathrm{k} = \int_{\mathrm{t}=0}^{t=t^*} P(t)v(t)dt \approx \sum P(t)\Delta d(t) \tag{2}$$

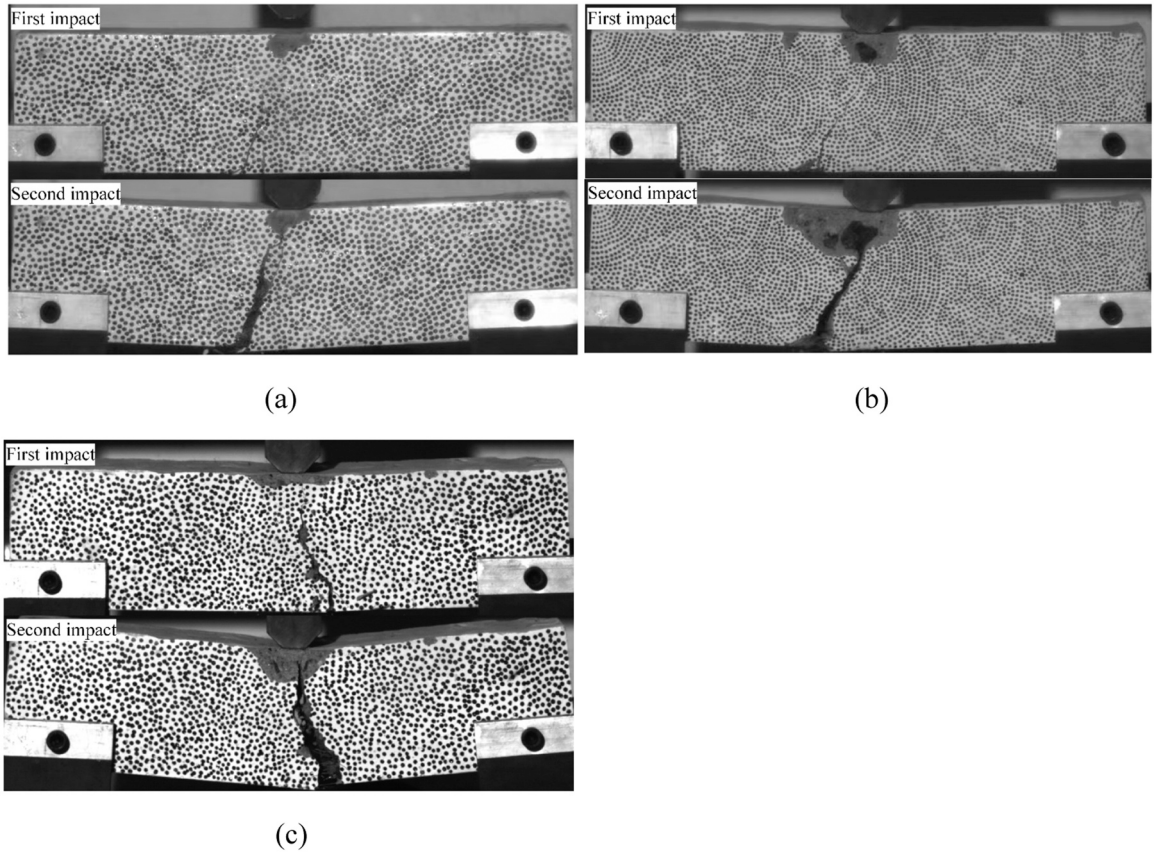

Fig. 5. The failure mode of SFCGC beams: (a) 0 %CGA-0.75 %SF-0.5 m; (b) 50 %CGA-0.75 %SF-0.5 m; (c) 100 %CGA-0.75 %SF-0.5 m.

Where $P(t)$ and $v(t)$ denote the time history of the impact force and the time history of the velocity when the specimen is hit by the falling drop-weight, respectively, and t^* is the duration of the impact event. U_k can also be determined by integrating the impact force-displacement curve.

3. Results and discussion

In the drop-weight impact test, 18 steel fiber-reinforced concrete beams with square cross-sections were subjected to the impact of a drop-weight. In this test, impact reaction force-time curves, displacement-time curves, and damage patterns of coal gangue concrete beams with steel fiber-reinforced were compared and discussed for different coal gangue replacement rate levels, steel fibers volume content, and weight drop heights. The damage process of steel fiber-reinforced coal gangue concrete beams (50 % CGA-0.75 % SF-0.5 m) under drop-weights impact is shown in Fig. 4.

3.1. The effect of CGA replacement rate on impact resistance of SFCGC beam

In order to demonstrate the effect of coal gangue replacement rate on beam damage patterns more intuitively, three types of beam damage patterns (0 %CGA-0.75 %SF-0.5 m, 50 %CGA-0.75 %SF-0.5 m, and 100 %CGA-0.75 %SF-0.5 m) were selected for discussion. As shown in Fig. 5, the higher the replacement rate of coal gangue in the concrete,

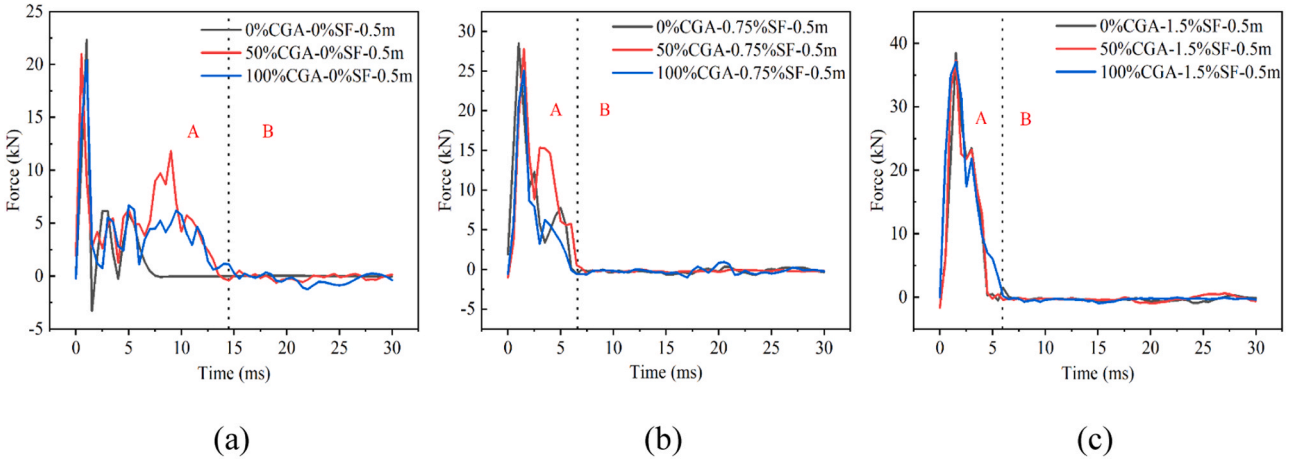

Fig. 6. Time History Curve of Impact Reaction Force at the first impact: (a) 0 %SF-0.5 m; (b) 0.75 %SF-0.5 m; (c) 1.5 %SF-0.5 m.

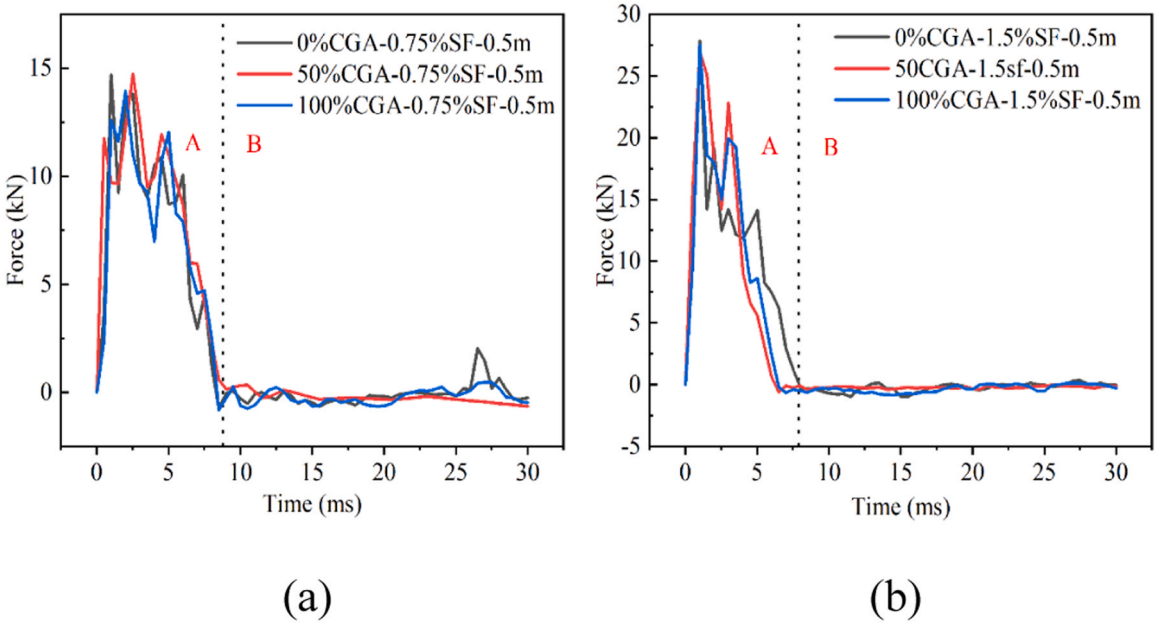

Fig. 7. Time History Curve of Impact Reaction Force at the second impact: (a) 0.75 %SF-0.5 m; (b) 1.5 %SF-0.5 m.

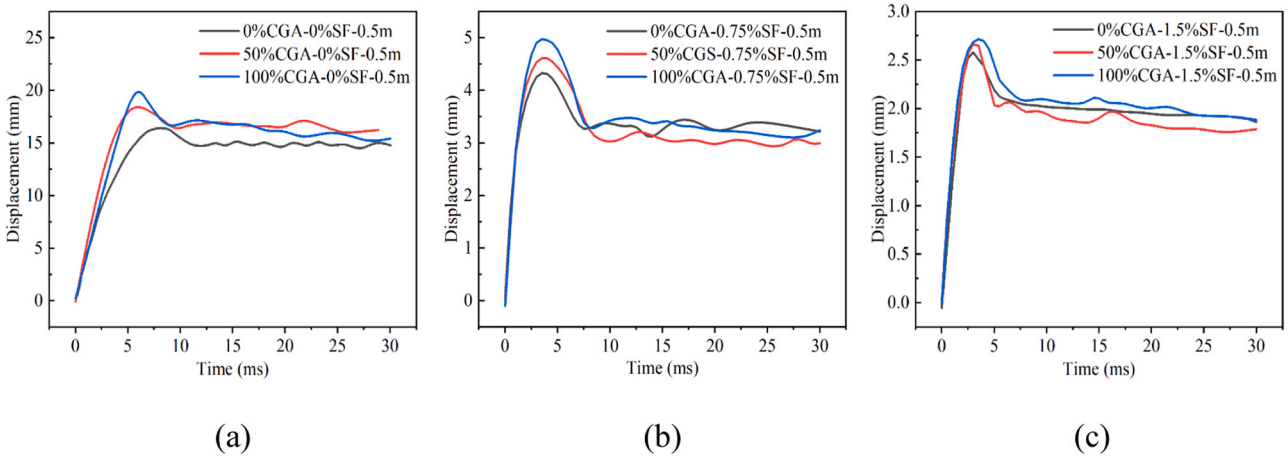

Fig. 8. Time History curve of Mid-span Displacement at the first impact: (a) 0 %SF-0.5 m; (b) 0.75 %SF-0.5 m; (c) 1.5 %SF-0.5 m.

the wider the cracks become after the first and second impacts, and the crack width increases dramatically after the second impact. Specifically, the crack widths of SFCGC beams with 0 %, 50 %, and 100 % CGA replacement rates are 1.08 mm, 1.14 mm, and 3.47 mm after the first impact, and the crack widths of beams are 7.18 mm, 11.96 mm, and 18.24 mm after the second impact.

Fig. 6 and Fig. 7 show the effect of the coal gangue replacement rate on the impact reaction force-time curve of the SFCGC beams at the first and second impacts. Each impact reaction force-time curve has approximately the same trend and is divided into an impact section (A) and a wave decay section (B). The SFCGC beam with a steel fiber volume content of 0 % failed after the first impact, and all other beams failed after the second impact. As shown in Fig. 6 and Fig. 7, the maximum reaction force rarely decreases if the CGA replacement rate is increased. When the SF volume content is 0 %, the CGA replacement rate increases the length of the impact section; when the SF volume content is 0.75 % and 1.5 %, the length of the impact section does not change significantly. Moreover, the maximum value of the reaction force during the second impact was significantly lower than the first impact.

Fig. 8 and Fig. 9 show the effect of the coal gangue replacement rate on the time curve of the SFCGC beam mid-span displacement at the first and second impacts. When the drop-weight is applied to the SFCGC beam, the energy generated by the impact is transferred from the drop-weight to the SFCGC beam. Part of the energy is dissipated by the specimen itself, resulting in local damage to the contact interface between the falling weight and the SFCGC beam, an increase in beam cracking, steel fiber tension and an overall bending deformation leading to a rapid increase in displacement. With the increase in displacement, the growth trend gradually slows down. After the displacement reaches its maximum value, the mid-span displacement of the beam undergoes a rebound phenomenon due to the elastic contraction of the steel fibers. Subsequently, the mid-span displacement of the beam gradually stabilizes at the residual displacement value. As can be seen in Fig. 8 and Fig. 9, increasing the replacement ratio of the coal gangue increases the peak and residual displacements of the midspan displacements of the SFCGC beams at the first and second impacts. The peak midspan displacement of the beams at the second impact increases significantly compared to the first impact. For example, when the SF volume content

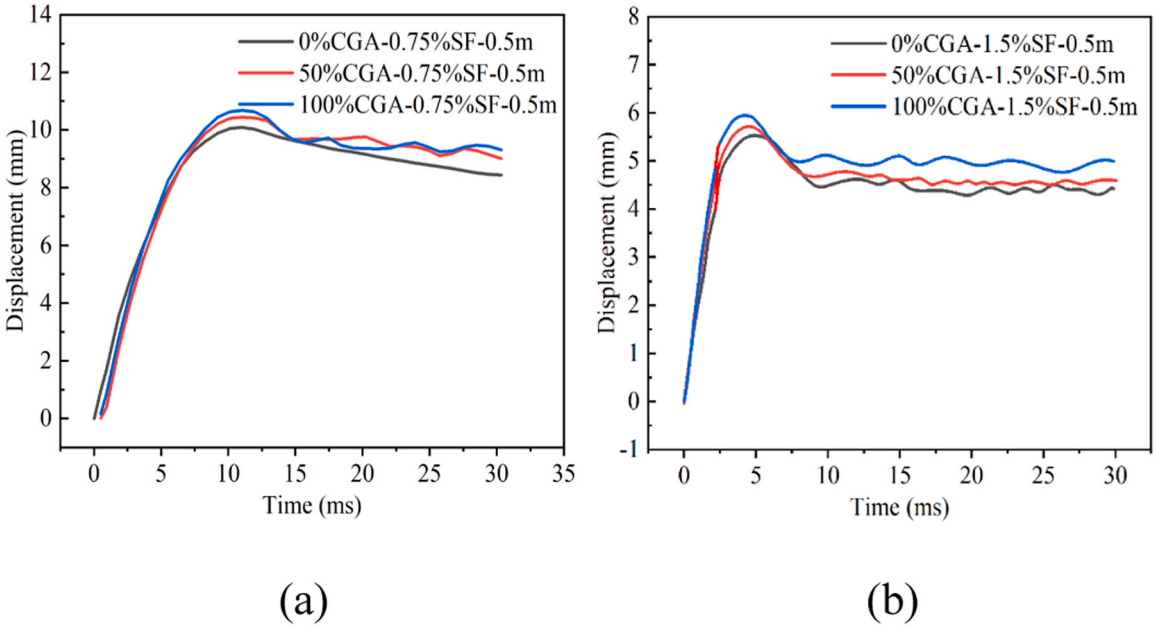

Fig. 9. Time history curve of Mid-span Displacement at the second impact: (a) 0.75 %SF-0.5 m; (b) 1.5 %SF-0.5 m.

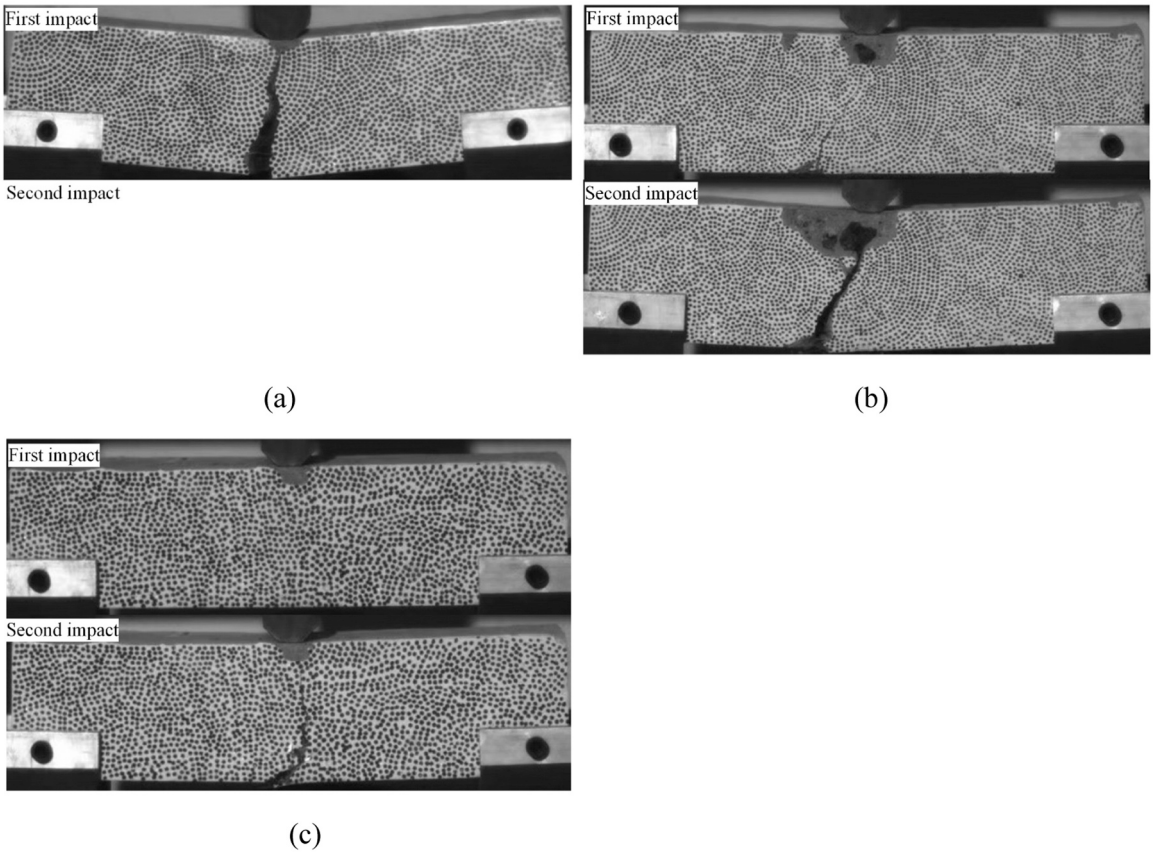

Fig. 10. The failure mode of SFCGC beams: (a) 50 %CGA-0 %SF-0.5 m; (b) 50 %CGA-0.75 %SF-0.5 m; (c) 50 %CGA-1.5 %SF-0.5 m.

is 0.75 %, the maximum mid-span displacements of SFCGC beams with 0 %, 50 %, and 100 % CGA replacement rates at the first impact are 4.33 mm, 4.61 mm, and 4.97 mm, respectively. The maximum mid-span displacements were 10.09 mm, 10.45 mm, and 10.68 mm for the second impact.

3.2. The effect of SF volume content on the impact performance of SFCGC beam

Fig. 10 shows the damage patterns of 50 %CGA-0 %SF-0.5 m, 50 % CGA-0.75 %SF-0.5 m, and 50 %CGA-1.5 %SF-0.5 m. As shown in Fig. 10(a), the CGC beams with 0 % steel fiber volume content were

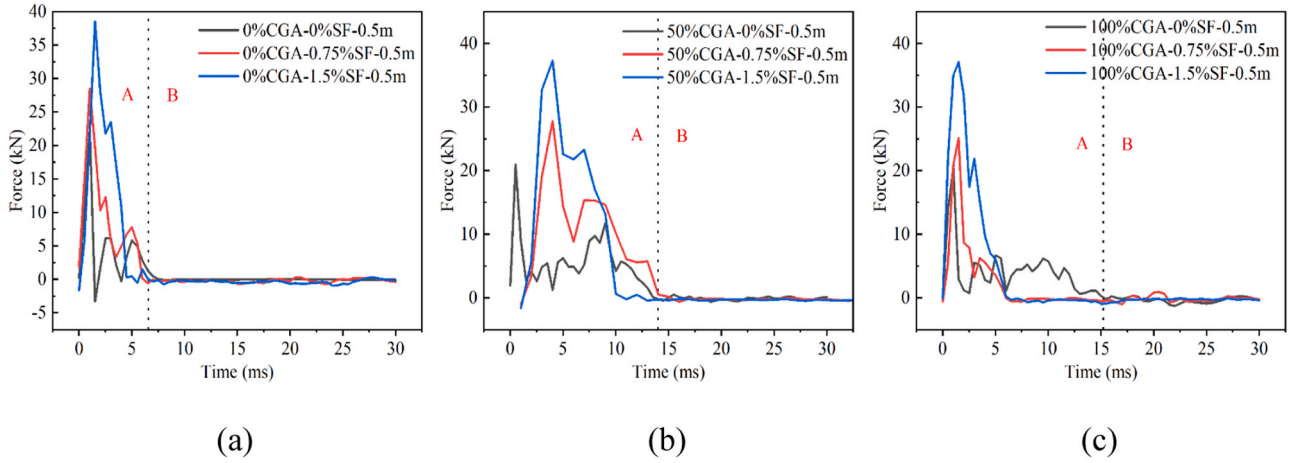

Fig. 11. Time History Curve of the Impact Reaction Force at the first impact: (a)0 %CGA-0.5 m; (b) 50 %CGA-0.5 m; (c) 100 %CGA-0.5 m.

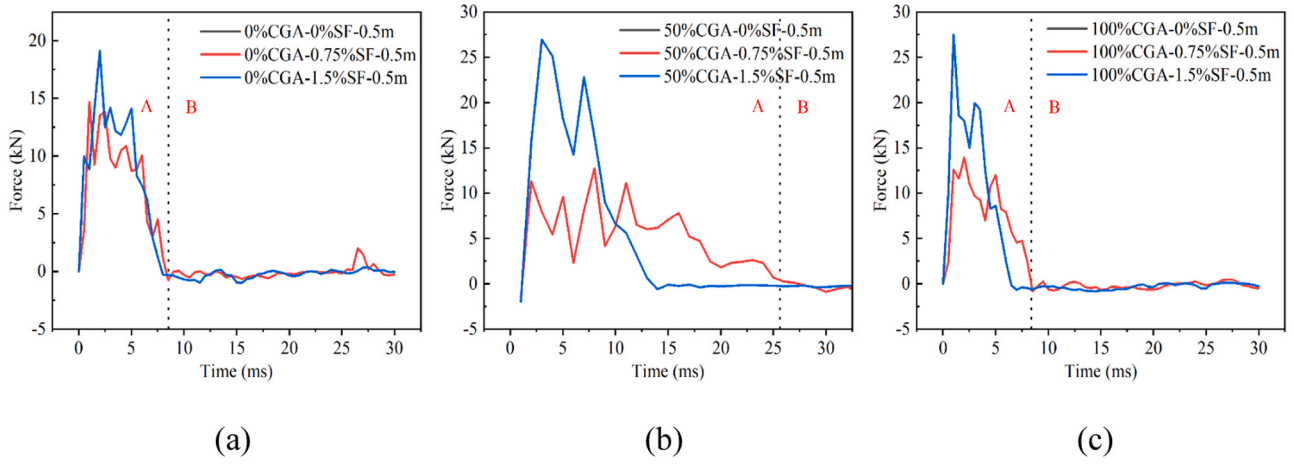

Fig. 12. Time History Curve of the Impact Reaction Force at the second impact: (a)0 %CGA-0.5 m; (b) 50 %CGA-0.5 m; (c) 100 %CGA-0.5 m.

fractured entirely after the first weight drop, so a second drop was not performed. Fig. 10 shows that after the first and second impacts, the higher the SF volume content, the smaller the crack caused by the impact, and the crack widens after the second impact. For example, SFCGC beams with 0.75 % and 1.5 % SF volume content had crack widths of 16.47 mm, 1.14 mm, and 0 mm after the first impact, and SFCGC beams with 0.75 % and 1.5 % SF volume content had crack widths of 11.96 mm and 5.65 mm after the second impact.

Fig. 11 and Fig. 12 show the effect of steel fiber volume content on the impact reaction force-time curves of SFCGC beams during the first and second impacts. During the first impact, the coal gangue concrete beam with 0 % SF volume content is directly shattered by the drop-weight, supporting a lower impact load. SFCGC beams with SF volume contents of 0.75 % and 1.5 % can withstand higher impact loads, and as

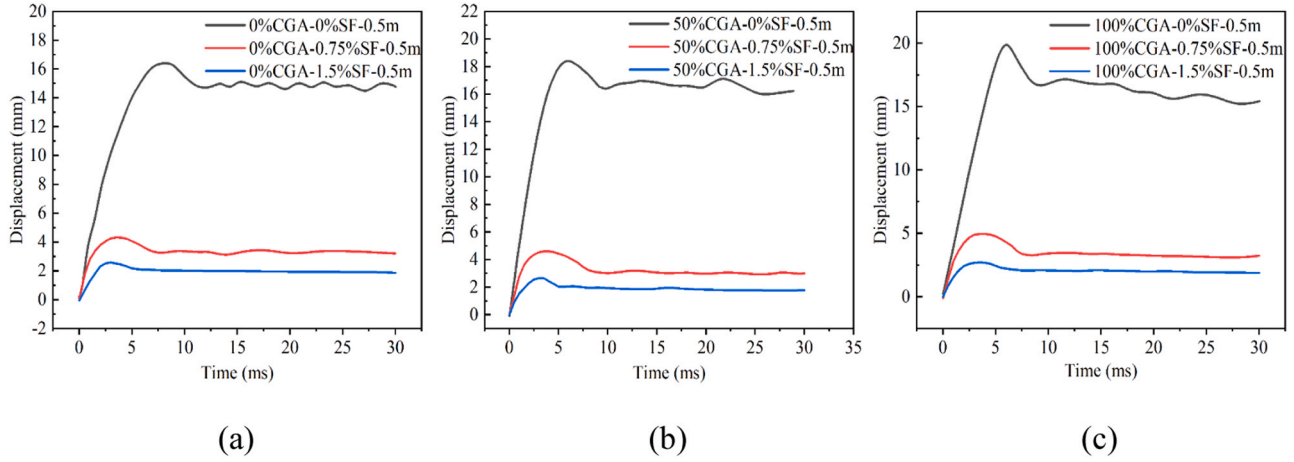

Fig. 13. Time History Curve of Mid-span Displacement at the first impact: (a)0 %CGA-0.5 m; (b) 50 %CGA-0.5 m; (c) 100 %CGA-0.5 m.

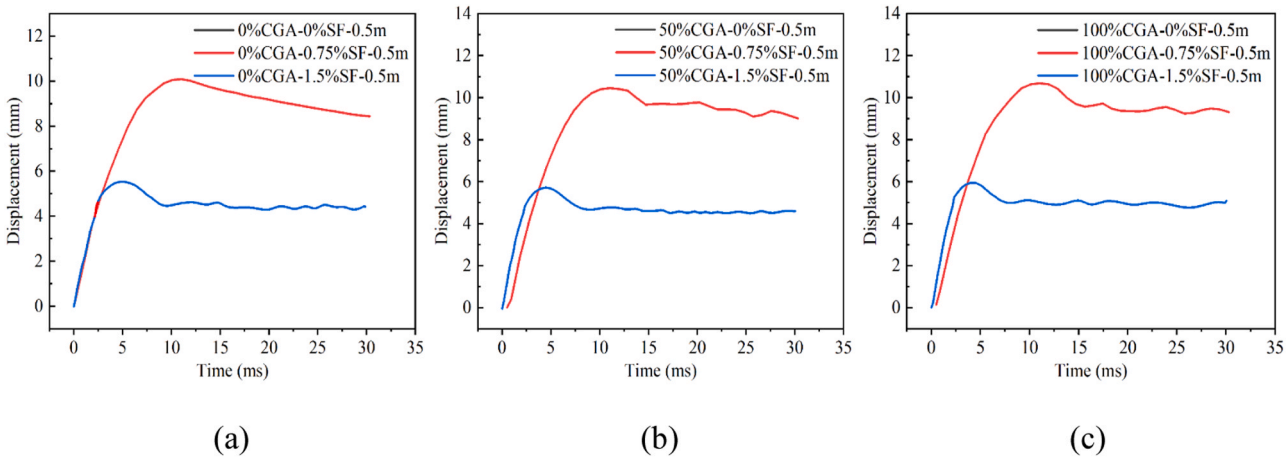

Fig. 14. Time History Curve of Mid-span Displacement at the second impact: (a)0 %CGA-0.5 m; (b) 50 %CGA-0.5 m; (c) 100 %CGA-0.5 m.

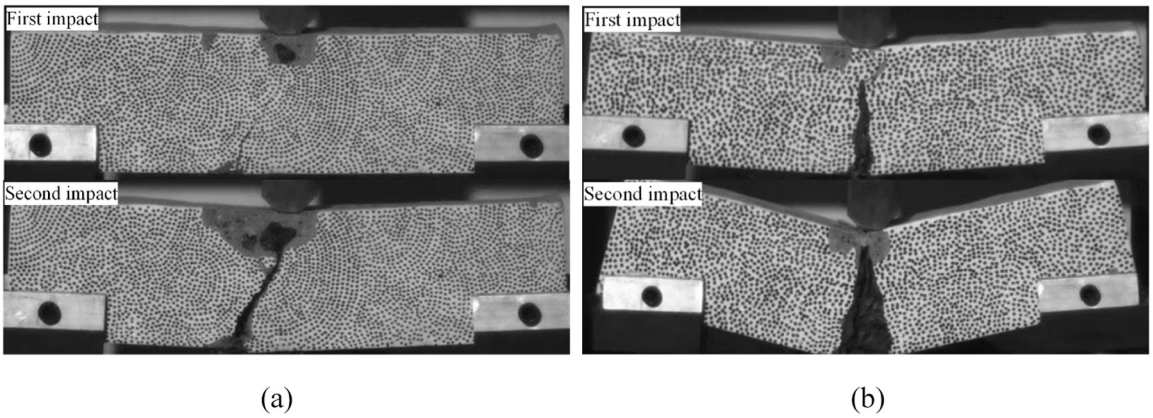

Fig. 15. The failure mode of SFCGC beams: (a) 50 %CGA-0.75 %SF-0.5 m; (b) 50 %CGA-0.75 %SF-1.0 m.

the SF volume content increases, so do the impact loads supported. Fig. 11 and Fig. 12 show that increasing the volume content of SF can considerably increase the maximum value of the impact reaction force of the SFCGC beam. In addition, increasing the volume content of SF can reduce the duration of the impact section. Since the first impact caused cracks on the surface of the beams, the SFCGC beams were subjected to a lower impact load during the second impact than during the first. For example, when the CGA replacement rate is 50 %, the maximum reaction forces of SFCGC beams with an SF volume content of 0 %, 0.75 %, and 1.5 %, are 21.00 kN, 27.79 kN, and 37.30 kN respectively during

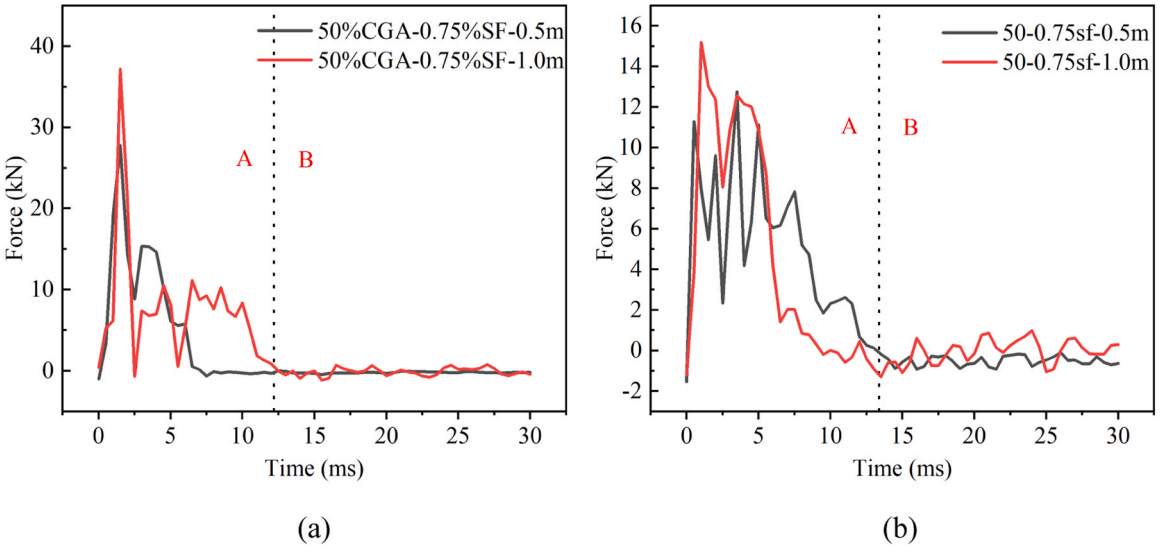

Fig. 16. Time History Curve of the Impact Reaction Forces: (a)First impact; (b)Second impact.

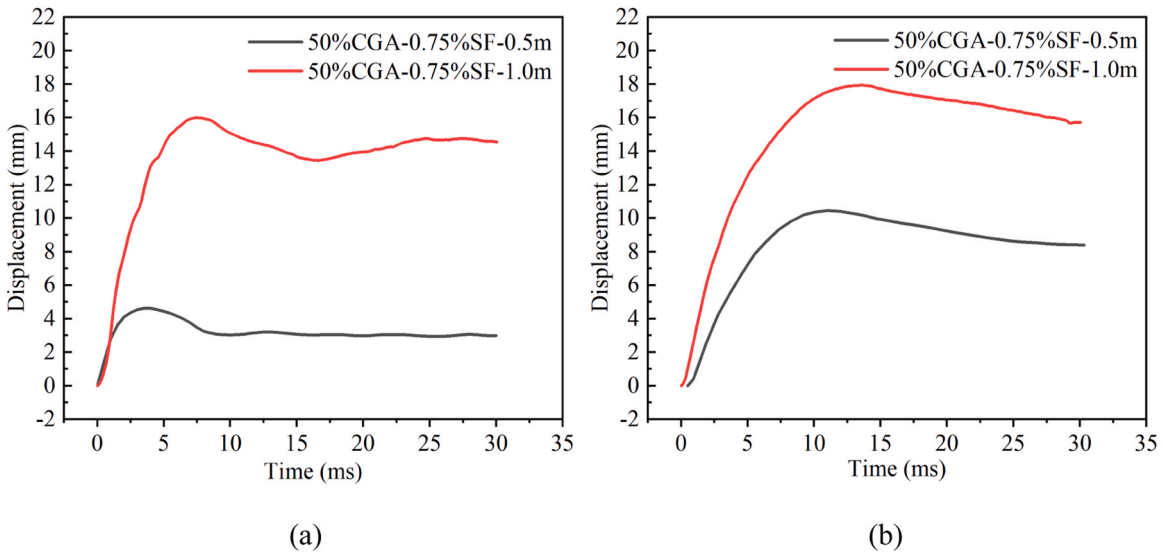

Fig. 17. Time History Curve of Mid-span Displacement: (a)First impact; (b)Second impact.

the first impact; during the second impact, the maximum reaction forces of SFCGC beams with an SF volume content of 0.75 % and 1.5 % are 12.76 kN and 26.98 kN respectively.

Fig. 13 and Fig. 14 show the effect of steel fiber volume content on the mid-span displacement curves of SFCGC beams during the first and second impacts. Increasing the SF volume content reduces the maximum mid-span and residual displacement at the first and second impacts, with the change from 0 % to 0.75 % particularly noticeable. In addition, the maximum displacement in the middle of the span at the second impact increased significantly compared to the first impact. For example, when the coal gangue replacement ratio is 50 %, the maximum displacement in the middle span of the SCCGC beams with a volume content of SF of 0 %, 0.75 %, and 1.5 % is 18.41 mm, 4.61 mm, and 2.66 mm, respectively, at the first impact. The maximum displacement in the middle span of the SCCGC beams with a volume content of SF of 0.75 %, and 1.5 % is 10.45 mm and 5.72 mm, respectively, at the second impact.

3.3. Impact resistance of SFCGC beams under 0.5 m and 1.0 m drop height

Fig. 15 shows the damage patterns of SFCGTC beams subjected to impact loads at two drop-weight heights. Fig. 15 shows that the degree of beam damage caused by drop-weight increases with increasing drop height. This is demonstrated in particular by the fact that the crack width due to the impact of the drop-weight increases with increasing drop height.

Fig. 16 shows the effect of the drop height of the drop-weight on the time course curve of the impact reaction force for the SFCGC beam impacts during the first and second impacts. As the impact height increases, the peak value of the reaction force becomes more significant, but the duration of the impact section decreases. For example, the peak reaction forces of the SFCGC beams during the first impact were 27.79 kN and 37.22 kN for the 0.5 m and 1.0 m drop heights, respectively, and 12.76 kN and 15.2 kN for the second impact, respectively.

Fig. 17 shows the effect of drop-weight drop height on the time history curves of the midspan displacements of the SFCGC beams at the first and second impacts. Increasing the drop-weight drop height increases the maximum midspan and residual displacement at the first and second impact. In particular, the maximum mid-span displacements of 50 % CGA-0.75 % SF are 4.61 mm and 15.99 mm at the first impact and 10.45 mm and 17.95 mm at the second impact for drop height of 0.5 m and 1.0 m, respectively.

Table 5
Summary of experimental parameters.

Specimen type	Drop height (m)	U_i (J)	Max force (kN)	Max deflection (mm)	U_k (J)	β
CG0-F0	0.5	73.5	22.35	16.41	47.49	0.65
	1.0	147	28.73	25.34	123.14	0.84
CG0-F0.75	0.5	73.5	28.51	4.33	61.36	0.83
	1.0	147	34.18	14.58	134.14	0.91
CG0-F1.5	0.5	73.5	38.51	2.58	50.17	0.68
	1.0	147	40.88	5.11	128.11	0.87
CG50-F0	0.5	73.5	21.01	18.41	48.53	0.66
	1.0	147	25.07	29.96	116.83	0.79
CG50-F0.75	0.5	73.5	27.79	4.61	53.10	0.72
	1.0	147	37.22	15.99	141.30	0.96
CG50-F1.5	0.5	73.5	37.30	2.66	46.71	0.64
	1.0	147	39.09	5.12	126.40	0.86
CG100-F0	0.5	73.5	20.40	19.86	49.44	0.67
	1.0	147	24.79	38.36	117.85	0.80
CG100-F0.75	0.5	73.5	25.10	4.97	57.92	0.79
	1.0	147	31.18	17.19	138.98	0.95
CG100-F1.5	0.5	73.5	37.09	2.71	66.38	0.90
	1.0	147	35.56	5.37	122.73	0.83

3.4. Energy absorption under impact

Calculate the input energy U_i according to Eq. (1). Assuming that there is no friction in the falling process of the drop-weight along the guide rail, i.e., U_d= 0. Define the parameter β as the ratio of absorbed energy U_k to input energy U_i, which can represent the energy absorption efficiency of the sample when subjected to the impact of the falling hammer, as shown in Eq. (3).

$$\beta = \frac{U_k}{U_i} \tag{3}$$

Table 5 summarises the mean values of the test parameters in the impact tests.

Fig. 18 shows the effects of the drop height, the CGA substitution rate, and the SF volume content on the energy absorbed by the SFCGC beams. It can be seen that the energy absorbed by all SFCGC beams increases with increasing drop height. In contrast, the CGA substitution rate has almost no effect on the energy absorption of the SFCGC beams,

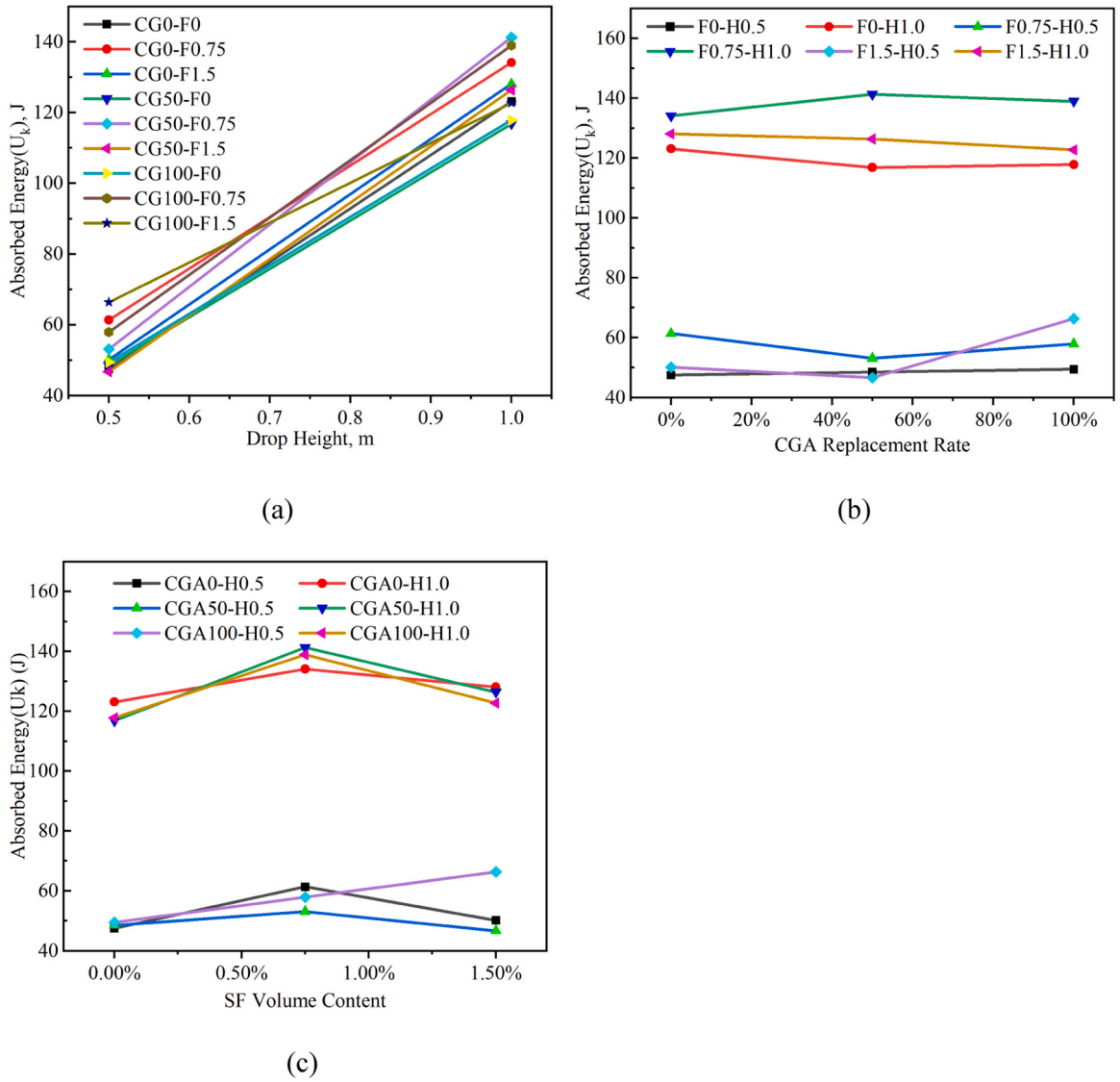

Fig. 18. Absorbed energy by impact: (a)U_k-Drop Height Curve; (b) U_k -CGA Replacement Rate Curve; (c) U_k -SF Vlume Content Curve.

reflecting the excellent performance of the gangue. The highest energy absorption for SFCGC beams was observed at a steel fiber volume content of 0.75 %. The higher energy absorption for SFCGC beams with an SF volume content of 0.75 % compared to normal concrete beams was predictable. However, the admixture of 1.5 % SF in CGA concrete can lead to the development of invisible microcracks inside the specimens, and this unfavorable phenomenon manifests itself when the specimens are subjected to impact. After the first impact, the energy absorbed by the specimens was only a fraction of the input energy, even though all 18 sets of beams exhibited large cracks. This is because some of the energy was dissipated by the friction of the drop-weight on the guide rail during the fall, and some of the energy remained in the system.

Fig. 19 shows the change in β with drop height, CGA substitution rate, and SF volume content, respectively. It can be seen that Fig. 19 shows results similar to those of Fig. 18. The energy dissipation capacity of natural aggregate concrete (NAC) ranges from 0.65 to 0.91 and that of CGC from 0.64 to 0.96, so CGC and NAC have similar energy dissipation capacities. The energy dissipation capacity of fiber-reinforced concrete is 0.64–0.96 and 0.65–0.84 for concrete without SF; the energy dissipation capacity of concrete increases significantly if fibers are incorporated into the concrete; this is because the bridging effect of steel fibers can make it easier for the concrete to absorb energy.

4. Finite element modelling

A nonlinear explicit finite element finite element model of the SFCGC beam was developed using LS-DYNA software developed by Livermore Software Technologies Corporation (LSTC) [31–38]. The beam, drop-weight, and supports were modeled as solid elements, and the supports were fixed in the x, y, and z directions. Use a 15 kg T-hard steel as the drop weight. In order to reduce the analysis run time, the drop heights of the drop-weight were set to 0.5 m and 1.0 m according to the free-fall Eq. (4), and the impact velocities were set to v = 3.13 m/s and v = 4.43 m/s, respectively. Set the initial velocity of the drop weight by using the keyword INITIAL_VOLOCITY_GENERATION. The initial distance between the bottom of the drop-weight and the top of the concrete beam was set at 1 mm. The model is shown in Fig. 20.

$$v = \sqrt{2gh} \tag{4}$$

4.1. Material model

4.1.1. Concrete

In LS-DYNA, the material used for concrete is MAT_CSCM_CONCRETE [35,38]. A summary of the parameters is given in Table 6. Axial compressive strength was obtained from the test results.

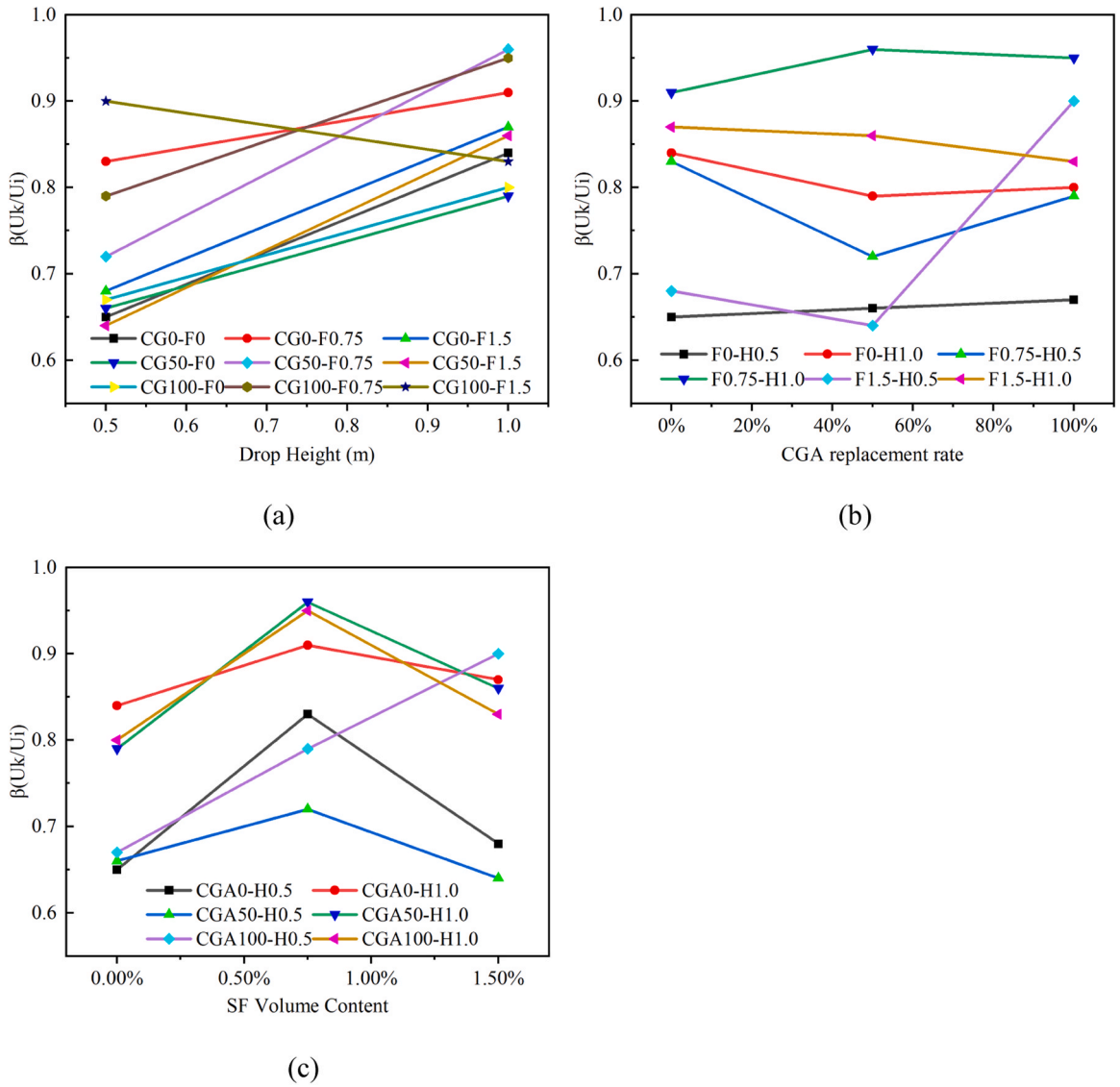

Fig. 19. Ratio of absorbed energy to the input potential energy for SFCGC specimens: (a) β-Drop Height Curve; (b) β -CGA Replacement Rate Curve; (c) β -SF Volume Content Curve.

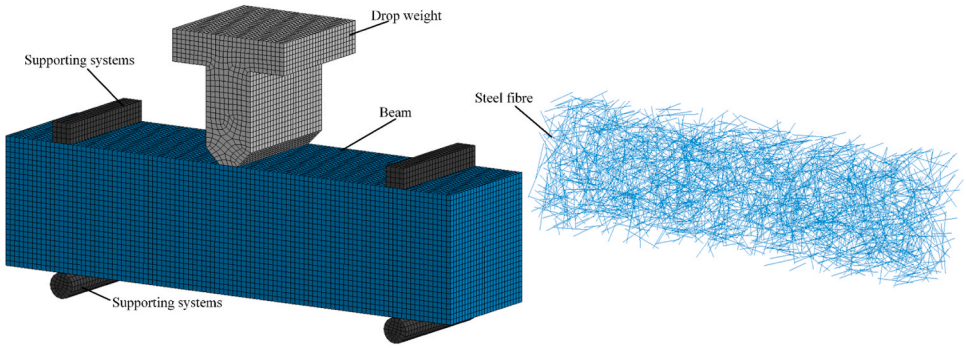

Fig. 20. LS-DYNA model.

4.1.2. Steel fiber

A self-programmed Python script was used to create the steel fiber model in the FEM of an SFCGC beam. Steel fibers are modeled using the isotropic elastoplastic model (keyword is *MAT_PLASTIC_KINEMATIC).

4.1.3. Supports and drop-weight

The material of the supports and drop-weight is MAT_RIGID. It is a rigid material, and no deformation of the material is taken into account. The density of the drop-weight and supports is 0.0078 g/mm^3 . The supports and the drop-weight have the same elastic modulus and Poisson's ratio, i.e., 2.05 × 105 MPa and 0.3, respectively. In addition, in

Table 6
Summary of data for material model MAT_CSCM_CONCRETE.

Name in LS-DYNA	Description	Value
RO	Density	0.00236 g/mm^3
IRATE	Rate effects options	1
IRETRC	Cap retraction option	0
PRED	Pre-existing damage	0
FPC	Axial compressive strength	f_c
DAGG	Maximum aggregate size	20 mm
UNITS	Units options	1

Note: Rate effects options = 1: Rate effects model turned on; Units options= 1; The system of unit is MPa, mm, msec, g/mm^3, N.

MAT_RIGID, boundary constraint can be applied directly to the supports or drop-weight, and the drop-weight retains the degree of freedom only in the y direction and cannot be moved or rotated in any other direction; the supports are fully restrained and cannot be moved or rotated in any direction. If the keyword (*CONTACT_FORCE_TRANSDUCER_PENALTY_ID) is added to the k-file, the time curve of the impact force can be obtained in post-processing.

4.2. Strain rate effect

The properties of concrete and steel fiber depend on strain rate (ε), and their strength increases when subjected to high strain rates (e.g.,

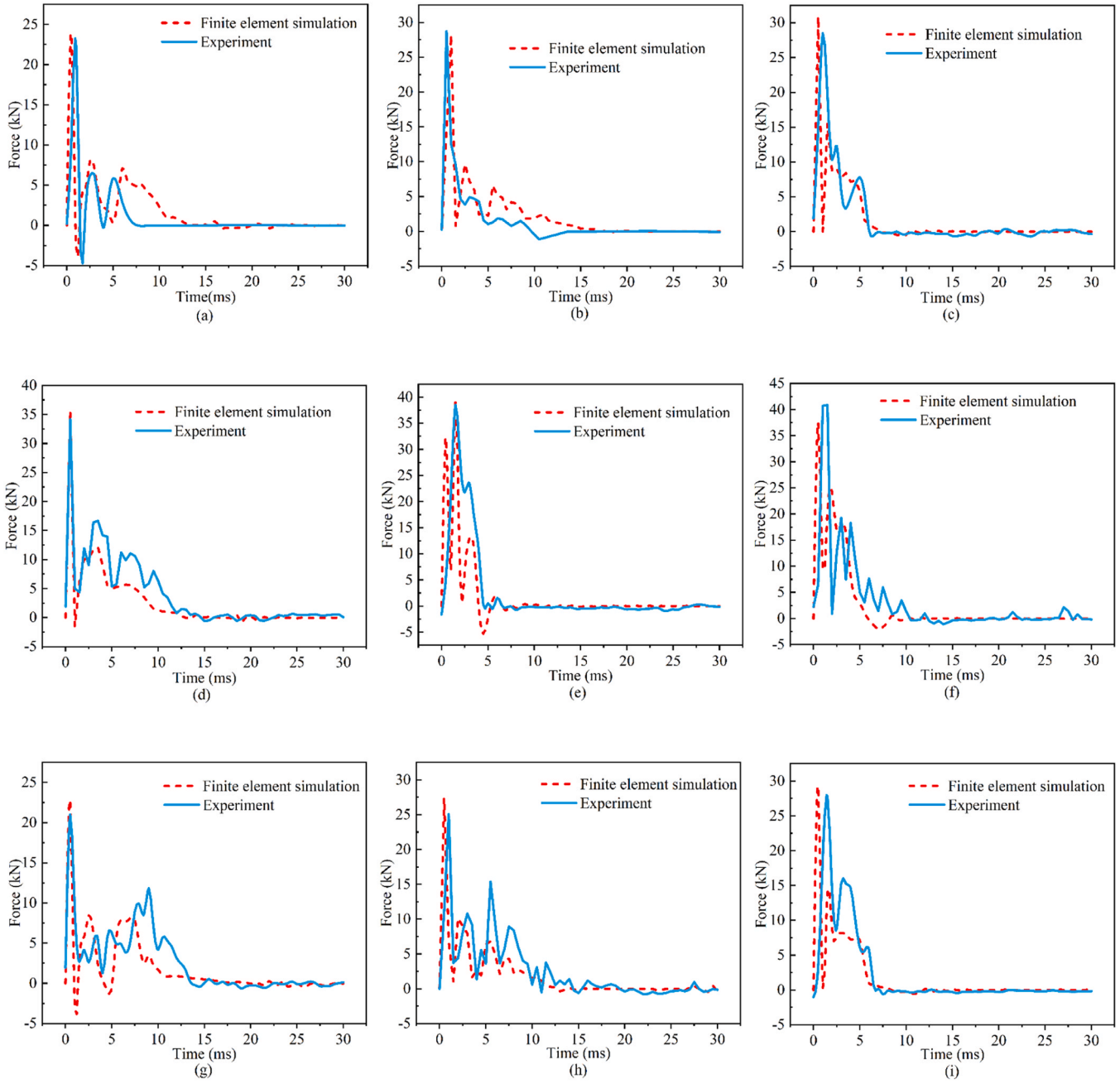

Fig. 21. Comparison of impact reaction force-time curves from tests and finite element simulations:(a)0 %CGA-0 %SF-0.5 m; (b) 0 % CGA – 0 %SF-1.0 m; (c) 0 % CGA – 0.75 %SF-0.5 m; (d) 0 % CGA – 0.75 %SF-0.5 m; (e) 0 % CGA – 1.5 %SF-0.5 m; (f) 0 % CGA – 1.5 %SF-1.0 m; (g) 50 % CGA – 0 %SF-0.5 m; (h) 50 % CGA – 0 %SF-1.0 m; (i) 50 % CGA – 0.75 %SF-0.5 m; (j) 50 % CGA – 0.75 %SF-1.0 m; (k) 50 % CGA – 1.5 %SF-0.5 m; (l) 50 % CGA – 1.5 %SF-1.0 m; (m) 100 % CGA – 0 %SF-0.5 m; (n) 100 % CGA – 0 %SF-1.0 m; (o) 100 % CGA – 0.75 %SF-0.5 m; (p) 100 % CGA – 0.75 %SF-1.0 m; (q) 100 % CGA – 1.5 %SF-0.5 m; (r) 100 % CGA – 1.5 %SF-1.0 m.

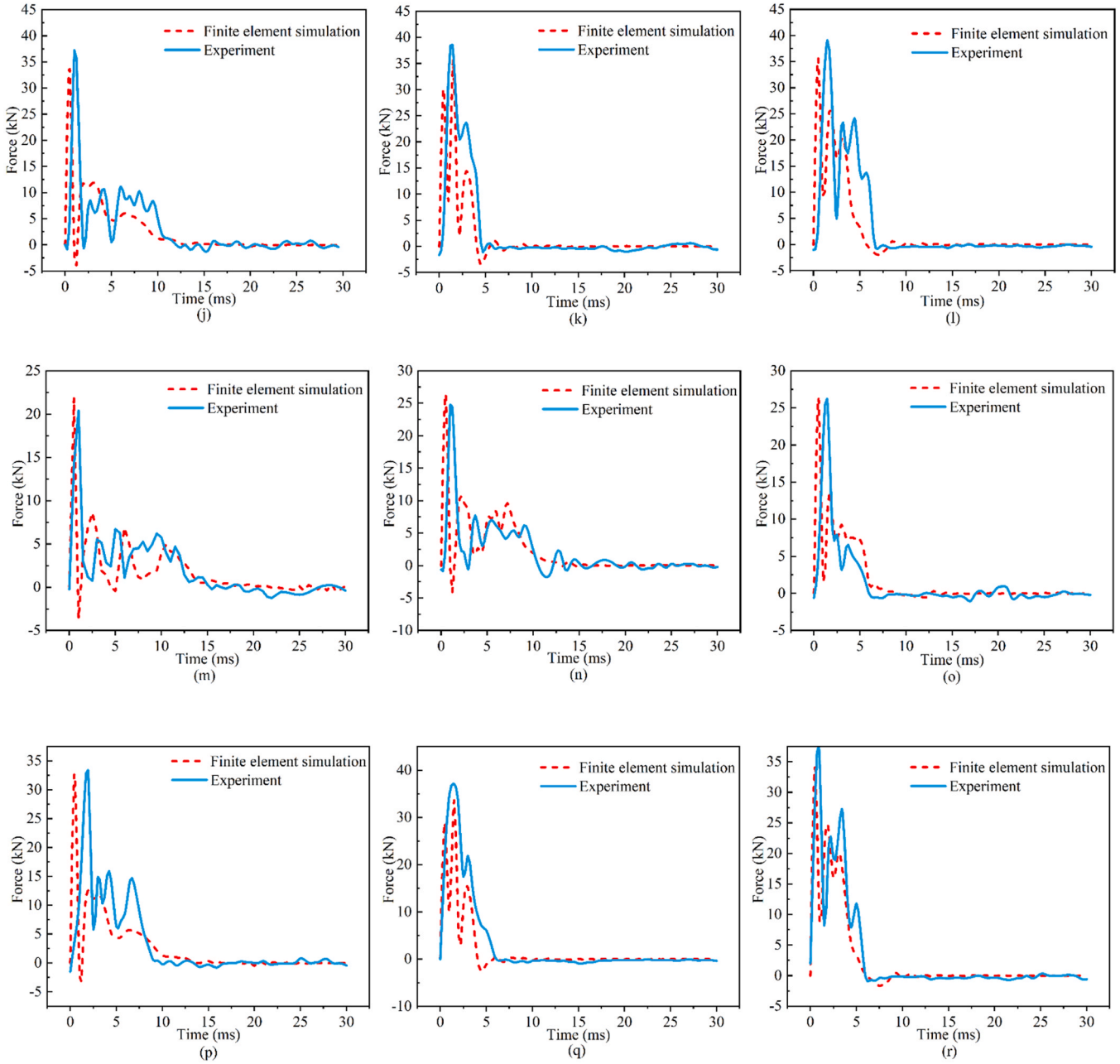

Fig. 21. (*continued*).

impact and blast loads) [31,32,35,36]. In the CSCM model, IRATE (rate effect options) = 1 is defined to consider the effect in strength through strain rate. The strain rate parameters SRC and SRP are defined for steel fiber materials and set to 0.04 and 5, respectively. Due to the isotropic properties of steel fibers, their corresponding strength enhancement under impact loading can be captured by the Cowper and Symonds model [42], which defines the scaling effect of the strain rate on the yield stress using Eq. (5).

$$DIF = \left(\frac{\varepsilon}{10^{-4}}\right)^{\alpha} \tag{5}$$

Where DIF is the dynamic increase factor, an essential parameter for measuring the rate sensitivity of the material, ε is strain rate (1/s), α is calculated according to Eq. (6).

$$\alpha = 0.074 - 0.04\left(\frac{f_y}{414}\right) \tag{6}$$

4.3. Solution control and database

Solution controls, including energy, hourglass, termination time, and time step, were determined sequentially to generate stable solutions for nonlinear finite element dynamics analyses. The hourglass coefficient was set to 0.14. A runtime limit of 30 ms was used in the keyword for the analysis completion time. The calculation time step was set to 0.5 ms with the keyword *DATABASE_BINARY_D3PLOT. During post-processing, the beams' vertical displacement at the span's center was extracted with the History command, and the impact force values were extracted with the American Standard Code for Information Interchange (ASCII) file command.

4.4. Validation of finite element models

To validate the results of the drop-weight test, the finite element analysis will be checked and compared with the test data using three aspects: the time history curve of the impact reaction force, the time history curve of the mid-span displacement, and the damage model.

4.4.1. Time history curve of impact reaction force

Fig. 21 shows the time history curve of impact reaction force for 18 groups of beams modeled with finite elements and a comparison with the experimental results. It is evident that the impact occurs within about 30 ms and that the maximum impact reaction force occurs suddenly, followed by a low amplitude attenuation waveform. The finite element model calculation results agree well with the test results. Just like the test results, the addition of coal gangue makes the impact force of SFCGC beams smaller; steel fiber can increase the impact force of SFCGC beams, and this role increases with the increase of steel fiber volume content; the increase of hammer drop height, SFCGC beams can withstand the impact force. The results show that the finite element model can better predict the impact reaction force of SFCGC beams.

4.4.2. Time history curve of mid-span displacement

Using the proposed finite element method, the time history curve of displacements in the mid-span of the SFCGC beam was obtained, as

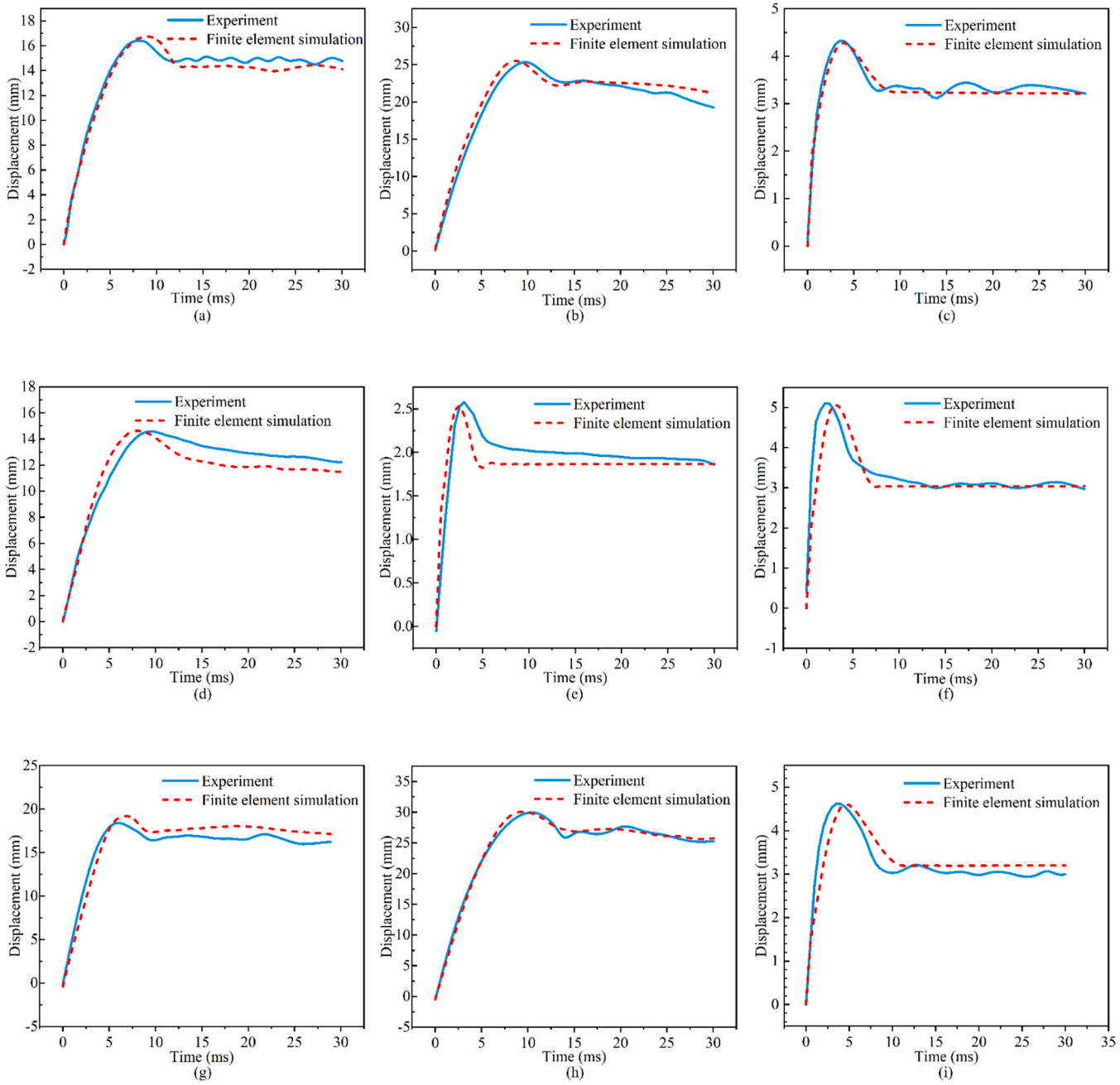

Fig. 22. Comparison of mid-span displacement-time curves from tests and finite element simulations: (a)0 %CGA-0 %SF-0.5 m; (b) 0 % CGA – 0 %SF-1.0 m; (c) 0 % CGA – 0.75 %SF-0.5 m; (d) 0 % CGA – 0.75 %SF-0.5 m; (e) 0 % CGA – 1.5 %SF-0.5 m; (f) 0 % CGA – 1.5 %SF-1.0 m; (g) 50 % CGA – 0 %SF-0.5 m; (h) 50 % CGA – 0 %SF-1.0 m; (i) 50 % CGA – 0.75 %SF-0.5 m; (j) 50 % CGA – 0.75 %SF-1.0 m; (k) 50 % CGA – 1.5 %SF-0.5 m; (l) 50 % CGA – 1.5 %SF-1.0 m; (m) 100 % CGA – 0 %SF-0.5 m; (n) 100 % CGA – 0 %SF-1.0 m; (o) 100 % CGA – 0.75 %SF-0.5 m; (p) 100 % CGA – 0.75 %SF-1.0 m; (q) 100 % CGA – 1.5 %SF-0.5 m; (r) 100 % CGA – 1.5 %SF-1.0 m.

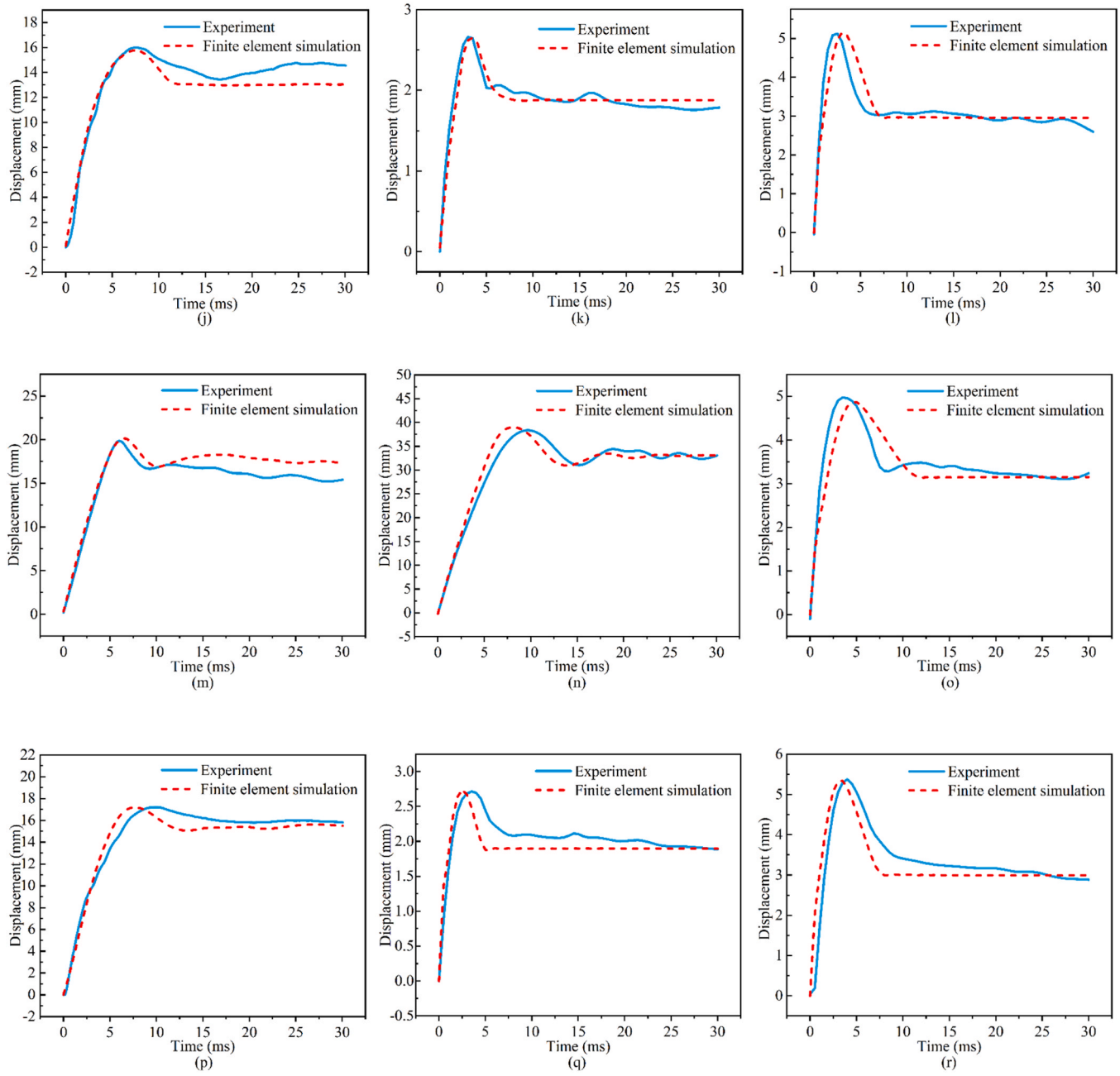

Fig. 22. (*continued*).

shown in Fig. 22. The simulation results agree with the test results. For example, the simulated value of the maximum mid-span displacement of the 0 %CGA-1.5 % SF-1.0 m beam is 14.5 mm, while it is 14.62 mm in the weight drop test, and the difference between the two values is about 0.83 %. Meanwhile, the simulation values of other beams differ from the test measurement results within 5 %. According to Fig. 22, it can be seen that adding coal gangue increases the span-to-span displacement; steel fibers can reduce the span-to-span displacement of SFCGC beams, and the higher the volume content of steel fibers, the smaller the mid-span displacement; increasing the drop height of drop-weight increases the span-to-span displacement of SFCGC beams. The results show that the finite element model can reasonably predict the mid-span displacement of SFCGC beams under the influence of drop-weight.

4.4.3. Failure mode

Fig. 23 shows the damage to the SFCGC beams in finite element modeling and testing, respectively. In addition to vertical cracks below the point of impact load application, the experimental samples also show localized damage at the point of impact load application. This was caused by the non-uniform top surface of the SFCGC beams used in the tests. Finite element modeling confirmed a similar damage pattern, namely vertical cracks extending downward from the middle of the span. In addition, finite element modeling revealed no localized failure at the exact point of impact load application.

5. Parametric study

Parametric analysis of SFCGC beams was carried out using finite element modeling. The effect of coal gangue replacement rate (0 %, 20 %, 40 %, 60 %, 80 %, and 100 %), steel fiber volume content (0 %, 0.5 %, 1.0 %, and 1.5 %), and drop height (0.5 m, 0.75 m and 1.0 m) on the impact resistance of SFCGC beams was investigated in order to gain a

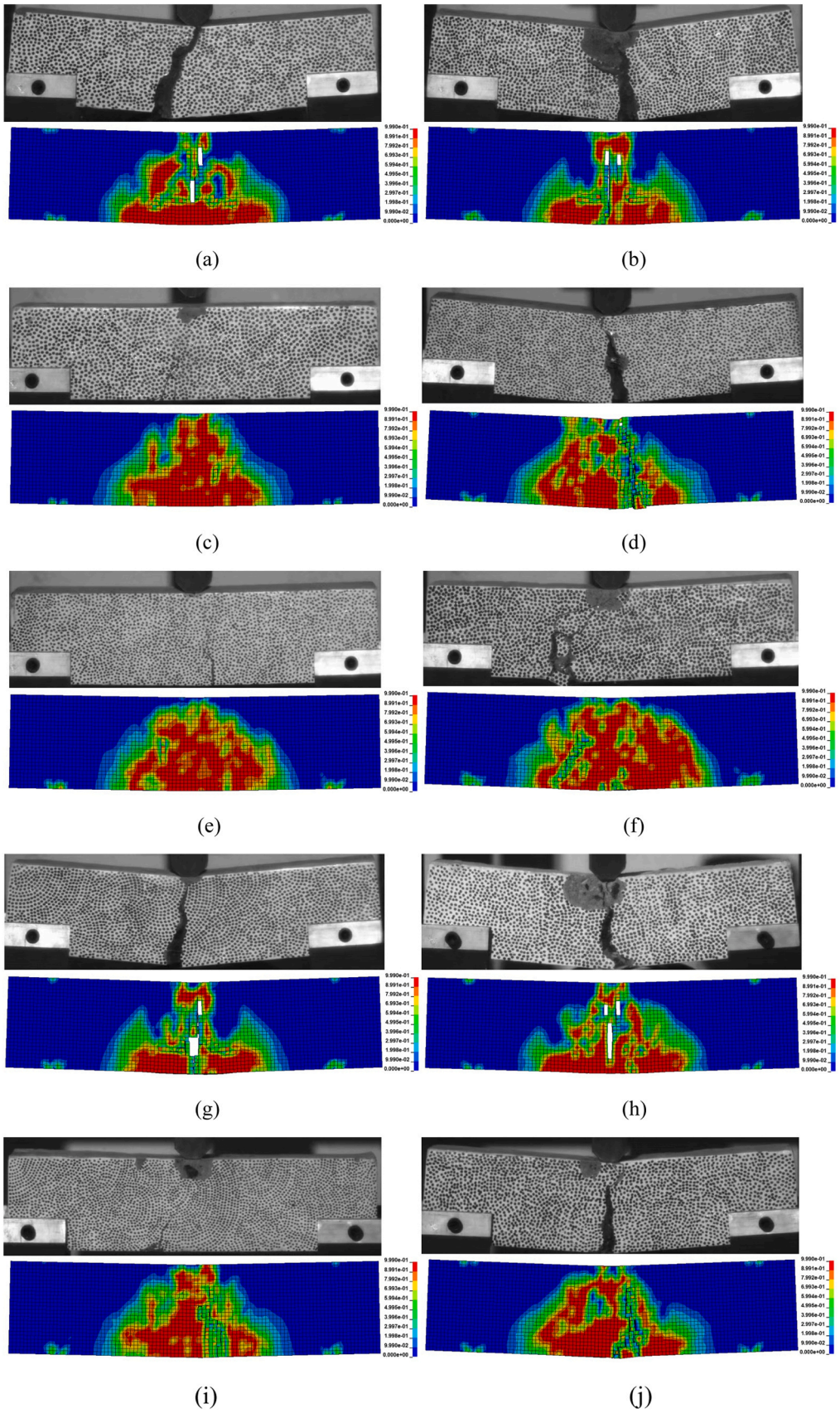

Fig. 23. Comparison of failure mode of beams in tests and finite element simulations: (a) 0 %CGA-0 %SF-0.5 m; (b) 0 %CGA-0 %SF-1.0 m; (c) 0 %CGA-0.75 %SF-0.5 m; (d) 0 %CGA-0.75 %SF-1.0 m; (e) 0 %CGA-1.5 %SF-0.5 m; (f) 0 %CGA-1.5 %SF-1.0 m; (g) 50 %CGA-0 %SF-0.5 m; (h) 50 %CGA-0 %SF-1.0 m; (i) 50 %CGA-0.75 %SF-0.5 m; (j) 50 %CGA-0.75 %SF-1.0 m; (k) 50 %CGA-1.5 %SF-0.5 m; (l) 50 %CGA-1.5 %SF-1.0 m; (m) 100 %CGA-0 %SF-0.5 m; (n) 100 %CGA-0 %SF-1.0 m; (o) 100 %CGA-0.75 %SF-0.5 m; (p) 100 %CGA-0.75 %SF-1.0 m; (q) 100 %CGA-1.5 %SF-0.5 m; (r) 100 %CGA-1.5 %SF-1.0 m;.

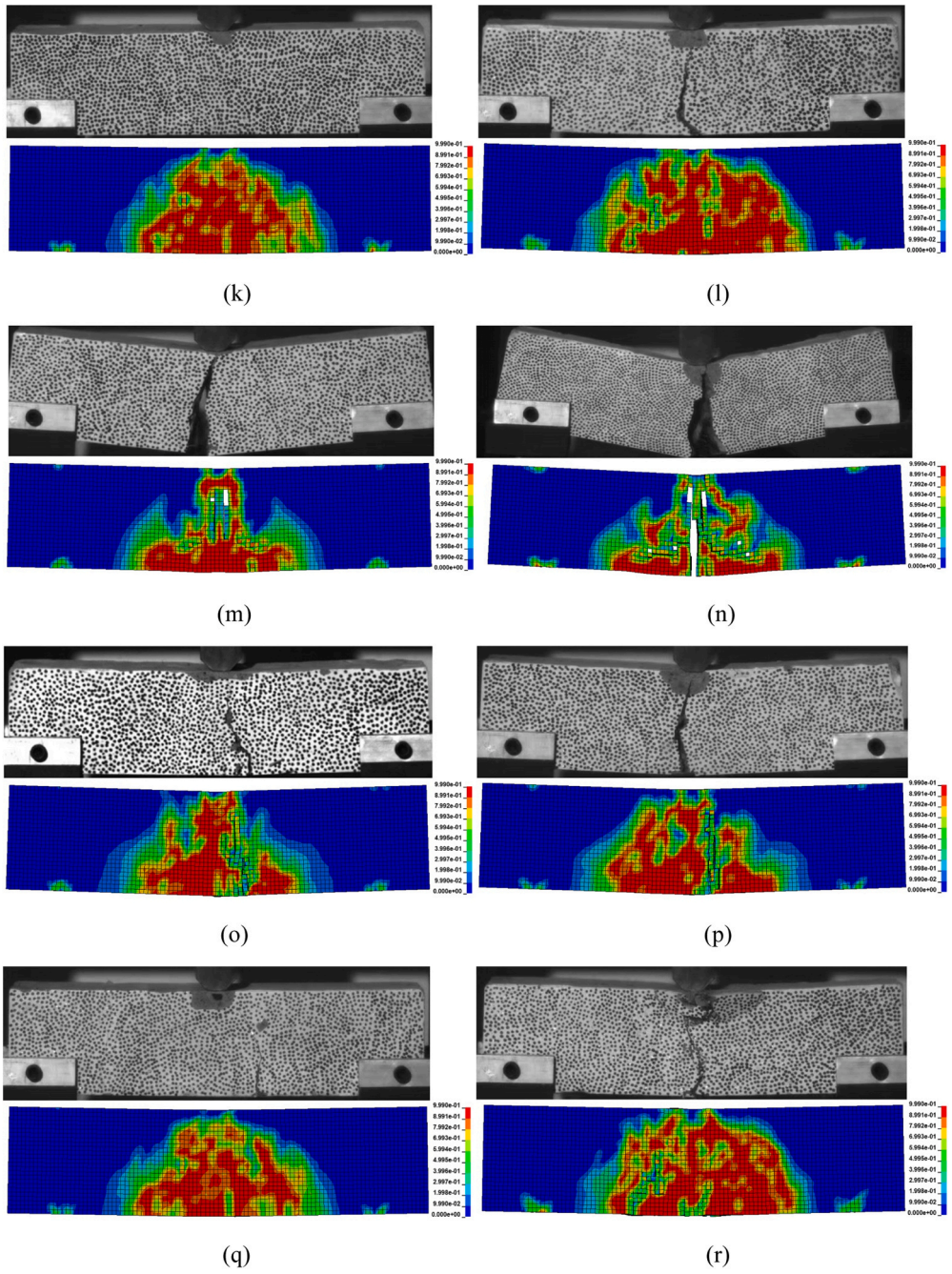

Fig. 23. (*continued*).

better understanding of the performance of SFCGC beams in the event of impact. Based on these three parameters, the finite element analysis results were extracted and discussed, i.e., impact reaction force-time, displacement-time, and effective plastic strain of the beams.

5.1. The effect of replacement ratio of CGA

Fig. 24(a) illustrates the variation of the impact reaction force-time curves with the CGA replacement rate for SFCGC beams. The maximum impact reaction force decreased by 4.88 %, 7.62 %, 9.86 %, 11.52 %, and 12.41 % as the CGA replacement rate increased from 0 % to 20 %, 40 %, 60 %, 80 %, and 100 %, respectively, indicating that the higher the CGA replacement rate, the lower the maximum reaction force of the SFCGC beam. Fig. 24(b) illustrates the variation of the displacement-time curve at the mid-span of the SFCGC beams with the CGA replacement rate. The maximum mid-span displacements increased by 3.89 %, 6.29 %, 11.38 %, 12.28 %, and 12.57 % when the CGA replacement rate increased from 0 % to 20 %, 40 %, 60 %, 80 %, and 100 %, respectively, indicating that the higher the CGA replacement rate, the higher the maximum mid-span displacements of the SFCGC beams.

To study the effect of the CGA replacement rate on the effective plastic strain, beams with an SF volume content of 1.0 % and a drop height of 0.5 m were selected, as shown in Fig. 25. Increasing the CGA replacement rate increased the damage of the SFCGC beams, but this damage did not increase significantly.

5.2. The effect of SF volume content

Fig. 26(a) shows the variation of the impact reaction force-time

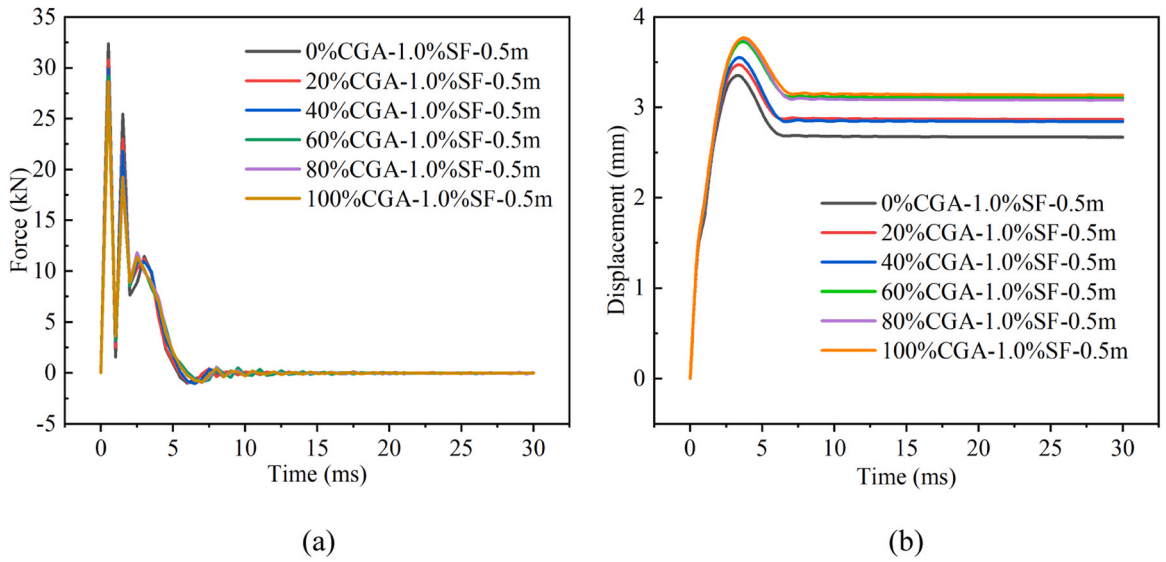

Fig. 24. The effect of CGA replacement rate on the time history curves of impact reaction force and displacement of SFCGC beams: (a) Impact Reaction Force-time curve; (a) Mid-span Displacement-time curve.

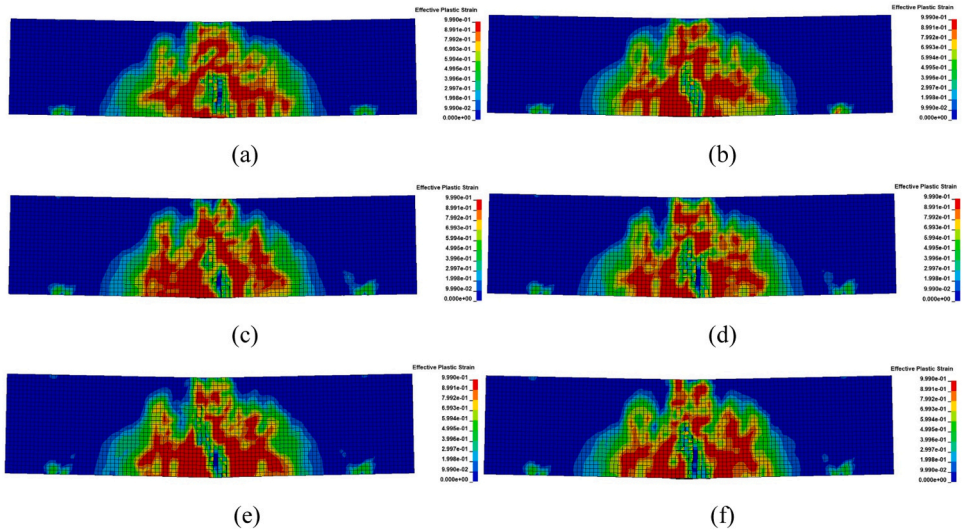

Fig. 25. The effect of CGA replacement rate on effective plastic strain in SFCGC beams: (a) CGA replacement rate= 0 %; (b) CGA replacement rate = 20 %; (c) CGA replacement rate = 40 %; (d) CGA replacement rate = 60 %; (e) CGA replacement rate = 80 %; (f) CGA replacement rate = 100 %.

curves of SFCGC beams with the SF volume content. The maximum impact load increased by 27.97 %, 34.60 %, and 40.97 % as the SF volume content increased from 0 % to 0.5 %, 1.0 %, and 1.5 %, respectively, suggesting that the SF volume content has a significant effect on the maximum impact load of SFCGC beams. Fig. 26(b) shows the variation of the mid-span displacement-time curves for SFCGC beams with SF volume content. The maximum mid-span displacements decreased by 49.45 %, 67.67 %, and 75.96 % when the SF volume content increased from 0 % to 0.5 %, 1.0 %, and 1.5 %, respectively, indicating that SF can effectively reduce the maximum mid-span displacements of SFCGC beams.

Beams with a coal gangue replacement rate of 40 % and drop height of 0.5 m were selected, and the effective plastic strain of beams with different SF volume contents was considered, as shown in Fig. 27. Increasing the SF volume content can make SFCGC beams reduce the damage effectively.

5.3. *The effect of the drop height of the drop-weight*

Fig. 28(a) shows the impact reaction force-time curves of the SFCGC beams as a relationship of the drop height of the drop-weight. The maximum impact reaction force increased by 4.82 % and 10.33 % when the drop height was increased from 0.5 m to 0.75 m and 1.0 m, respectively, indicating that the drop height significantly affects the maximum impact load of the SFCGC beam. Fig. 28(b) shows the mid-span displacement-time curves as a relationship of the drop height of the drop weight. When the drop weight was increased from 0.5 m to 0.75 m and 1.0 m, the maximum displacements at mid-span increased by 16.34 % and 27.32 %, indicating that the drop weight greatly influences the displacements at mid-span.

To analyze the effective plastic strain of SFCGC beams under different drop heights of the drop-weight, beams with coal gangue replacement degree of 40 % and SF volume content of 1.0 % were selected, as shown in Fig. 29. Increasing the drop height of the drop-weight resulted in more significant damage to the SFCGC beams.

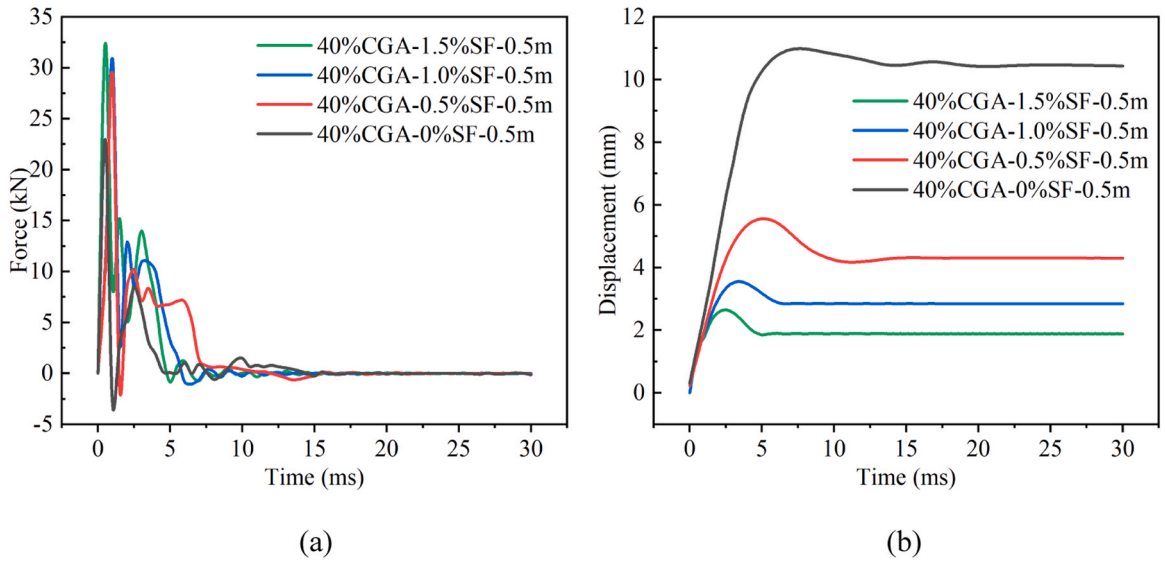

Fig. 26. The effect of SF volume content on the time history curves of impact reaction force and mid-span displacement of SFCGC beams: (a) Impact Reaction Force-time curve; (a) Mid-span Displacement-time curve.

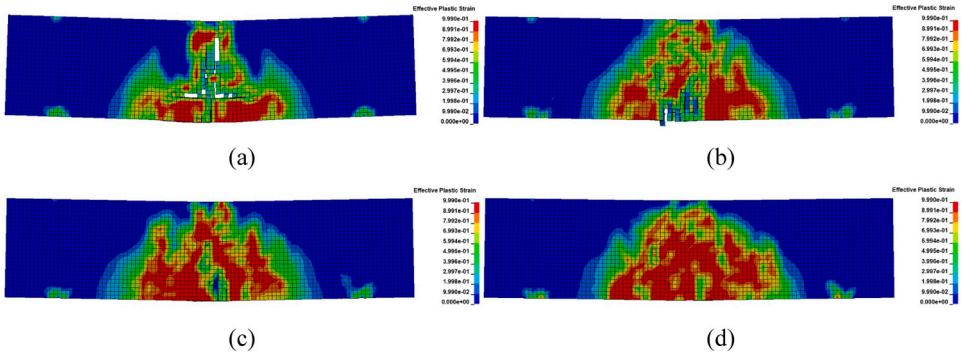

Fig. 27. The effect of SF volume content on effective plastic strain in SFCGC beams: (a) SF volume content= 0 %; (b) SF volume content = 0.5 %; (c) SF volume content = 1.0 %; (d) SF volume content = 1.5 %.

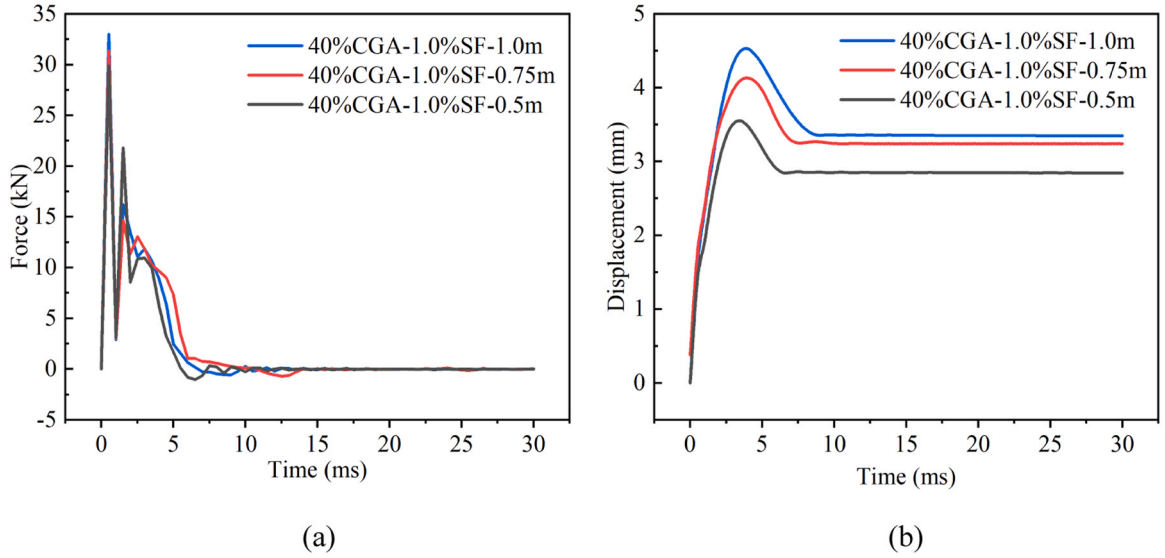

Fig. 28. The effect of drop height of the drop-weight on the time history curves of impact reaction force and mid-span displacement of SFCGC beams: (a) Impact Reaction Force-time curve; (a) Mid-span Displacement-time curve.

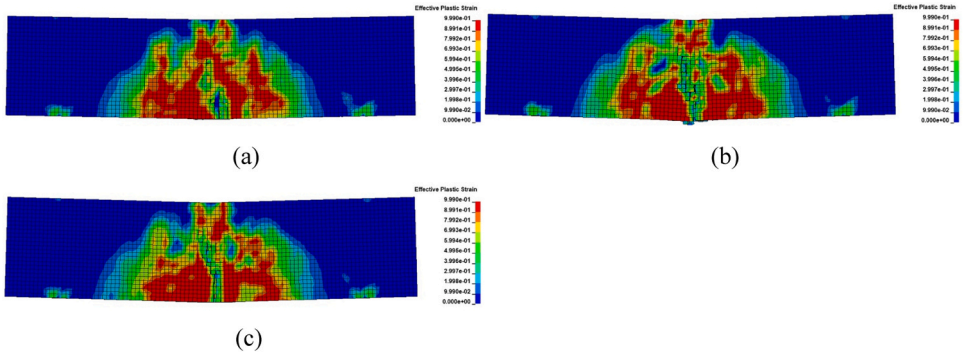

Fig. 29. The effect of drop height of the drop-weight on effective plastic strain in SFCGC beams: (a) Drop height= 0.5 m; (b) Drop height = 0.75 m; (a) Drop height = 1.0 m.

6. Conclusion

This paper investigates the static mechanical properties and impact resistance of steel fiber-reinforced coal gangue concrete (SFCGC). The variables investigated are coal gangue replacement ratio, steel fiber volume content, and drop height, and an experimental study and finite element analysis of the instrumented drop-weight impact were carried out. The essential conclusions drawn from this study are as follows:

1) The results of the drop-weight impact test show that CGA adversely affects the impact resistance, but this adverse effect is minimal, and SF can effectively improve the impact resistance of coal gangue concrete beams. Compared with ordinary concrete, the replacement ratios of 50 % and 100 % CGA reduce the maximum impact reaction force by 2.54 %~6.06 % and 3.69 %~12.33 %, respectively, while the maximum mid-span displacement increases by 3.22 %~12.19 % and 5.27 %~14.90 %, respectively. Compared with ordinary coal gangue concrete, the addition of 0.75 % and 1.5 % steel fiber increased the maximum impact reaction force by 23.05 %~32.34 % and 72.27 %~81.84 %, respectively, and the maximum mid-span displacement decreased by 73.62 %~74.96 % and 84.28 % ~86.33 %, respectively. In addition, increasing the drop height of the drop-weight increases the impact reaction force and the mid-span displacement of the beams, and the damage to the beams is more serious. Therefore, although the impact resistance of the new steel fiber-reinforced concrete is slightly lower than that of ordinary steel fiber-reinforced concrete, it is still applicable in engineering.
2) The reliability and accuracy of the developed finite element model were verified by comparing the finite element analysis results with the test results. The time history curves of impact reaction force and mid-span displacement obtained from the finite element analysis are consistent with the test results, and the failure modes of the beams are almost identical. This can serve as a basis for future impact tests.
3) A parametric study was conducted ~~based on~~ using the validated finite element model. The analysis shows that the higher the CGA replacement rate is, the worse the impact resistance of SFCGC is; the higher the volume content of SF is, the better the impact resistance of SFCGCD is. This study can serve as a reference for the use and design of future steel fiber-reinforced concrete under impact loading.
4) This study provides a basis for the future application of SFCGC. The experimental results and numerical calculations given in this paper can be served as a basis for determining the impact resistance of SFCGC beams in the design. The influence of different types of fibers on the dynamic properties of fiber-reinforced concrete under blast or impact loading requires further investigation.

Declaration of Competing Interest

The authors declare that they have no known competing financial interests or personal relationships that could have appeared to influence the work reported in this paper.

Data availability

Data will be made available on request.

Acknowledgments

This research was financially supported by Scientific research projects of Education Department of Jilin Province (JJKH20240381KJ), Scientific Research Project of Jilin Provincial Housing and Urban-Rural Development Department (2023-K-21), Jilin Provincial Science and Technology Development Plan Project (20220203082SF), and Natural Science Foundation of Guangxi Zhuang Autonomous Region, China (2022GXNSFAA035529). The authors wish to acknowledge the sponsors. However, any opinions, findings, conclusions and recommendations presented in this paper are those of the authors and do not necessarily reflect the views of the sponsors.

References

[1] Li J, Wang J. Comprehensive utilization and environmental risks of coal gangue: a review. J Clean Prod 2019;239:117946.
[2] Quero X, Izquierdo M, Monfort E, Alvarez E, Font O, Moreno T, et al. Environmental characterization of burnt coal gangue banks at Yangquan, Shanxi Province, China. Int J Coal Geol 2008;75(2):93–104.
[3] Haibin L, Zhenling L. Recycling utilization patterns of coal mining waste in China. Resour Conserv Recycl 2010;54(12):1331–40.
[4] Dong Z, Xia J, Fan C, Cao J. Activity of calcined coal gangue fine aggregate and its effect on the mechanical behavior of cement mortar. Constr Build Mater 2015;100:63–9.
[5] Huang G, Ji Y, Li J, Hou Z, Dong Z. Improving strength of calcinated coal gangue geopolymer mortars via increasing calcium content. Constr Build Mater 2018;166:760–8.
[6] Salguero F, Grande JA, Valente T, Garrido R, De la Torre ML, Fortes JC, et al. Recycling of manganese gangue materials from waste-dumps in the Iberian Pyrite Belt-Application as filler for concrete production. Constr Build Mater 2014;54:363–8.
[7] Yao Z, Fang Y, Kong W, et al. Experimental study on dynamic mechanical properties of coal gangue concrete. Adv Mater Sci Eng 2020;2020:1–16.
[8] Karimaei M, Dabbaghi F, Sadeghi-Nik A, Dehestani M. Mechanical performance of green concrete produced with untreated coal waste aggregates. Constr Build Mater 2020;233:117264.
[9] Gao S, Zhao G, Guo L, Zhou L, Yuan K. Utilization of coal gangue as coarse aggregates in structural concrete. Constr Build Mater 2021;268:121212.
[10] Li D, Song X, Gong C, Pan Z. Research on cementitious behavior and mechanism of pozzolanic cement with coal gangue. Cem Concr Res 2006;36(9):1752–9.
[11] Zhang N, Sun H, Liu X, Zhang J. Early-age characteristics of red mud–coal gangue cementitious material. J Hazard Mater 2009;167(1–3):927–32.
[12] Yi C, Ma H, Zhu H, Li W, Xin M, Liu Y, et al. Study on chloride binding capability of coal gangue based cementitious materials. Constr Build Mater 2018;167:649–56.
[13] Ma H, Zhu H, Wu C, Chen H, Sun J, Liu J. Study on compressive strength and durability of alkali-activated coal gangue-slag concrete and its mechanism. Powder Technol 2020;368:112–24.
[14] Zhou M, Dou Y, Zhang Y, et al. Effects of the variety and content of coal gangue coarse aggregate on the mechanical properties of concrete. Constr Build Mater 2019;220:386–95.

[15] Qiu J, Zhou Y, Vatin NI, et al. Damage constitutive model of coal gangue concrete under freeze-thaw cycles. Constr Build Mater 2020;264:120720.
[16] Luo D, Wang Y, Zhang S, Niu D, Song Z. Frost resistance of coal gangue aggregate concrete modified by steel fiber and slag powder. Appl Sci 2020;10(9):3229.
[17] Zhang Y, Ling TC. Reactivity activation of waste coal gangue and its impact on the properties of cement-based materials-a review. Constr Build Mater 2020;234:117424.
[18] Hu Q, Fang G. Study on mechanical properties of recycled concrete block mixed with coal gangue and plant fiber. IOP Conf Ser Earth Environ Sci 2020;508(1):012179.
[19] Teng S, Afroughsabet V, Ostertag CP. Flexural behavior and durability properties of high performance hybrid-fiber-reinforced concrete. Constr Build Mater 2018;182:504–15.
[20] Wang Z, Zhao N. Properties of steel fiber reinforced coal gangue coarse aggregate concrete. Wuhan Univ J Nat Sci 2014;19(3):262–8.
[21] Hao Y, Hao H, Jiang GP, et al. Experimental confirmation of some factors influencing dynamic concrete compressive strengths in high-speed impact tests. Cem Concr Res 2013;52:63–70.
[22] Hao Y, Hao H, Chen G. Experimental investigation of the behaviour of spiral steel fibre reinforced concrete beams subjected to drop-weight impact loads. Mater Struct 2016;49:353–70.
[23] Omidinasab F, Moazami Goodarzi S, Sahraei Moghadam A. Characterization and optimization of mechanical and impact properties of steel fiber reinforced recycled concrete. Int J Civ Eng 2022;20:41–55.
[24] Moghadam AS, Omidinasab F, Dalvand A. Flexural and impact performance of functionally graded reinforced cementitious composite (FGRCC) panels. Struct 2021;29:1723–33.
[25] Zhuang J, Ni P, Chen J, et al. Study on the impact resistance of steel fiber-reinforced self-compacting concrete after high temperature. Struct 2023;57:105281.
[26] Vivas JC, Zerbino R, Torrijos MC, et al. Effect of the fibre type on concrete impact resistance. Constr Build Mater 2020;264:120200.
[27] Abid SR, Abdul-Hussein ML, Ayoob NS, et al. Repeated drop-weight impact tests on self-compacting concrete reinforced with micro-steel fiber. Heliyon 2020;6(1).
[28] Almusallam TH, Abadel AA, Al-Salloum YA, et al. Effectiveness of hybrid-fibers in improving the impact resistance of RC slabs. Int J Impact Eng 2015;81:61–73.
[29] Abid SR, Gunasekaran M, Ali SH, et al. Impact performance of steel fiber-reinforced self-compacting concrete against repeated drop weight impact. Crystals 2021;11(2):91.
[30] Almusallam T, Abadel A, Siddiqui N, et al. Impact behavior of hybrid-fiber reinforced concrete beams. Struct 2022;39:782–92.
[31] Derseh SA, Urgessa G, Mohammed TA. Finite element analysis of the response of conventional and special reinforcement detailed concrete beams subjected to impact loads. Struct 2023;52:57–82.
[32] Pham T.T., Kurihashi Y., Masuya H. Impact response of reinforced concrete beam with cushion using finite-element analysis. Case Stud in Constr Mater 2022;17:e01147.
[33] Jönsson J., Stenseke A. Concrete Beams Subjected to Repeated Drop-Weight Impact and Static Load-Assessment of structural response in experimental testing and predicted response with numerical analyses. 2018.
[34] Fan W, Zhong Z, Huang X, et al. Multi-platform simulation of reinforced concrete structures under impact loading. Eng Struct 2022;266:114523.
[35] Wei J, Li J, Wu C, et al. Impact resistance of ultra-high performance concrete strengthened reinforced concrete beams. Int J Impact Eng 2021;158:104023.
[36] Li H, Chen W, Hao H. Dynamic response of precast concrete beam with wet connection subjected to impact loads. Eng Struct 2019;191:247–63.
[37] Yu Y, Lee S, Cho JY. Deflection of reinforced concrete beam under low-velocity impact loads. Int J Impact Eng 2021;154:103878.
[38] Abadel A, Abbas H, Siddiqui N, et al. Numerical investigation of projectile impact behavior of hybrid fiber-reinforced concrete slabs. Case Stud Constr Mater 2023;19:e02533.
[39] ACI Committee 544. Measurement of properties of fiber reinforced concrete (ACI 544.2R-89), Farmington hills, MI, USA: American Concrete Institute; 1989.
[40] GB/T 50081-2019. Standard for test methods of concrete physical and mechanical properties. Beijing: China Architecture & Building Press; 2019.
[41] GB/T 50080-2016. Standard for test method of performance on ordinary fresh concrete. Beijing: China Architecture & Building Press; 2016.
[42] Lstc. LS-DYNA theory manual. Livermore, California: Livermore Software Technology Corporation (LSTC); 2019.
[43] Wang L, Zhang J, Chen W, et al. Short term crack width prediction of CFRP bars reinforced coral concrete. Eng Struct 2020;218:110829.
[44] Yang Y F, Fu F, Bie X M, et al. Axial compressive behaviour of CFDST stub columns with large void ratio. J. Constr. Steel Res 2021;186:106892.
[45] Cai B, Xu L F, Fu F. Shear resistance prediction of post-fire reinforced concrete beams using artificial neural network. Int J Concr Struct M 2019;13(1):46.
[46] Cai B, Pan G, Fu F. Prediction of the postfire flexural capacity of RC beam using GA-BPNN machine learning. J Perform Constr Facil 2020;34(6):04020105.